www.sciencemag.org/content/355/6323/385/suppl/DC1

Supplementary Materials for

Airborne laser-guided imaging spectroscopy to map forest trait diversity and guide conservation

G. P. Asner,* R. E. Martin, D. E. Knappm, R. Tupayachi, C. B. Anderson,† F. Sinca, N. R. Vaughn, W. Llactayo

*Corresponding author. Email: gpa@carnegiescience.edu

Published 27 January 2017, *Science* **355**, 385 (2017)
DOI: 10.1126/science.aaj1987

This PDF file includes:

Materials and Methods

Approach

Our mapping and analysis approach is based on airborne laser-guided imaging spectroscopy to derive wide-area coverage data on seven canopy foliar traits, in this case sampling a total of 2,045,379 ha distributed across 76 million ha of the Peruvian Andes-Amazon region. Imaging spectroscopy data are combined with climatic and geophysical data using a geospatial modeling approach to provide spatially explicit model-based estimates of canopy foliar traits and their relationships with biophysical factors throughout the study region (**Fig. S1**). An overview of the methodology depicted in Fig S1 is as follows: (a) A pre-stratification step combines geologic, soil, vegetation type, elevation, and forest cover maps to forecast the potential range of environmental conditions to be encountered during airborne surveys. (b) The country is gridded into sampling cells, and the Carnegie Airborne Observatory (CAO) is used to sample each grid cell, yielding samples of canopy functional traits. CAO flightlines are 1.2 km wide with a spatial resolution of 2.0 m. (c) An array of satellite data is compiled and processed to provide continuous geographic information on topographic and climate variables at 1.0 ha grid cell resolution. (d) The geospatial maps and CAO data are integrated using a geostatistical modeling approach based on Random Forests Machine Learning (RFML) to map canopy foliar traits at one-hectare resolution, along with spatially-explicit uncertainty.

Airborne canopy trait mapping

We sampled the forested portion of the Peruvian Andes-Amazon region using the Carnegie Airborne Observatory (CAO) (*30*). Pre-stratification of the region was carried out to guide a spatially robust acquisition of airborne samples relative to surface geology (*31*), elevation (NASA Shuttle Radar Topography Mission), and a forest ecosystems map of Peru (*32*). The forested portion of the Peruvian Andes and Amazon basin was gridded into 100 km x 100 km sectors, and the CAO was flown to randomly sample an average 3% of each grid cell (equating to about 30,000 ha per 100 x 100 km sector). The final airborne sampling totaled 2,045,379 ha of direct observations (**Fig. S2**).

The CAO instruments used for this study include a high-fidelity Visible-to-Shortwave Infrared (VSWIR) imaging spectrometer and a dual laser, waveform Light Detection and Ranging (LiDAR) scanner. We collected the data from an altitude of 2000 m (± 250 m) above ground level (a.g.l.), an average flight speed of 60 m s^{-1}, and a mapping swath of 1.2 km. The VSWIR spectrometer measures spectral radiance in 427 channels spanning the 350-2510 nm wavelength range in 5 nm increments (full-width at half-maximum). The spectrometer has a 34° field-of-view and an instantaneous field-of-view of 1 mrad. From 2000 m a.g.l., the spectral data were collected at 2.0 m ground sampling distance, or pixel size, throughout the region. The LiDAR has a beam divergence set to 0.5 mrad, and was operated at 200 kHz with 17^{o} scan half-angle from nadir, providing swath coverage similar to the spectrometer. The LiDAR point density for this mapping study was four laser shots m^{-2}. The total number of spectral and LiDAR samples was 5.11 and 20.45 billion, respectively.

The LiDAR data were used to precisely geolocate the spectral data in three dimensions. To achieve this, the laser ranges were combined with embedded high resolution Global Positioning System-Inertial Measurement Unit (GPS-IMU) data to determine the 3-D locations of laser returns, producing a 'cloud' of LiDAR data. The LiDAR data cloud consists of a large number of georeferenced point elevation estimates, where elevation is determined relative to a reference ellipsoid. We used these points to interpolate a raster digital terrain model (DTM) for the ground surface of each landscape. This was achieved using a 10 m x 10 m kernel, with the lowest elevation estimate in each kernel assumed to be ground. Subsequent points were evaluated by fitting a horizontal plane to each of the ground seed points. If the closest unclassified point was < 5.5° and < 1.5 m higher in elevation, it was classified as ground. The digital surface model (DSM) was based on interpolations of all first-return points. Measurement of the vertical difference between the DTM and DSM yielded a digital canopy model (DCM) of vegetation height above ground.

A standardized GPS-based pulse-per-second measurement recorded within the VSWIR data was used to precisely co-locate the spectral imagery to the LiDAR DSM. A camera model, created in the laboratory and refined for the flight installation, was used to determine the three-dimensional location and field-of-view of each sensor element, which was combined with the standardized timing information for data co-registration of the data sources. Prior to converting the VSWIR observations to canopy trait estimates, the spectral data were radiometrically corrected from raw DN values to radiance (W sr^{-1} m^{-2} nm^{-1}) using a flat-field correction, radiometric calibration coefficients and spectral calibration data collected in the laboratory prior to flight. The geometry data from the VSWIR-LiDAR data fusion steps were used to atmospherically correct the radiance imagery using a modified version of the ACORN-5 model (Imspec LLC, Glendale, CA USA). To improve aerosol corrections in ACORN-5, the model was iteratively run with different visibilities until the reflectance at 420 nm (which is relatively constant for vegetated pixels) is less than 1% (*33*). Reflectance imagery was corrected for cross-track brightness gradients using a bidirectional reflectance distribution function (BRDF) modeling approach. A 1-ha sample of lowland Peruvian Amazon forest is shown in **Fig. S3** to indicate the precision co-alignment of VSWIR and LiDAR data.

The chemometric method for converting VSWIR spectra to estimates of canopy foliar chemical traits and LMA was developed and validated in Asner et al. (*21*). The method provides automated processing of VSWIR data over large geographic areas, while minimizing localized effects of varying sun-sensor-canopy geometry, inter- and intra-crown shading, forest gaps, land use, and terrain-related artifacts. This data-fusion approach, called laser-guided imaging spectroscopy (*34*), is facilitated by the collection of boresight-aligned VSWIR and LiDAR measurements. The approach removes pixels unsuitable for sunlit canopy spectroscopic analysis, including non-canopy surfaces, shaded canopy pixels, and pixels with low foliar content (**Fig. S4**) (*21*). To achieve this, the LiDAR was used to measure the height of the vegetation within each spectral pixel, and only vegetation taller than 2 m in height was considered. Additionally, we detect and remove pixels containing inter-canopy shade using a ray-tracing model (*34*). To further ensure that remaining spectral pixels contain sufficient foliar cover for chemometric

analysis, a minimum Normalized Difference Vegetation Index (NDVI) threshold of 0.8 is also applied. Spectral pixels that met these three criteria were considered suitable for canopy trait analysis, and those spectra were averaged at a mapping resolution of 1 ha.

Following preparation of the filtered 1-ha resolution spectra, we convolved the data to 10-nm bandwidth and applied a brightness-normalization adjustment (*35*). This reduced the contribution of varying leaf area index (LAI) to chemometric determinations of foliar traits from remotely sensed data (*36*). The resulting spectra were trimmed at the far ends (400 nm, 2500 nm) of the measured wavelength range, as well as in regions dominated by atmospheric water vapor (1350-1480, 1780-2032 nm) that blocks a spectral reflectance signal. We used calibration equations derived from Partial Least Squares Regression (PLSR; *37*) analysis validated by Asner et al. (*21*) to convert the 1-ha resolution spectral data to foliar canopy chemicals (N, P, Ca, Phenols, Lignin, Water) and LMA. The PLSR approach is beneficial because it utilizes the continuous spectrum as a single measurement rather than in a band-by-band type of analysis (*38, 39*). The spectral dependence and variance of canopy traits is shown in **Fig. S5**. Across 79 1-ha field plots in Peru, Asner et al. (*21*), showed that functional foliar chemical traits (N, P, Ca, Phenols, Lignin, Water, and LMA) could be predicted with accuracies ranging from 5-18% root mean square error (RMSE) of their mean values **(Table S1)**.

Geospatial Modeling

We used the Random Forest Machine Learning algorithm (RFML; *40*) to model the spatial relationship between the seven foliar traits derived from airborne laser-guided imaging spectroscopy and a suite of spatially extensive biogeophysical and climatological data sets. RFML is a computational machine-learning approach that fits multiple decision trees to geospatially-coincident environmental datasets using a random subset of the input variables for each tree constructed for the airborne canopy trait samples. The modal value of the calculated decision trees is used to create an "ensemble" tree that is used for prediction. RFML is non-parametric, robust to data skew, and allows for a large number of variable inputs (*41*). This approach has been used extensively to scale remotely sensed estimates of forest structure, biomass, and traits to regional levels (e.g., *42*). Unique to this modeling approach, categorically-specified vegetation maps are not used as input, thus avoiding the commonly used paint-by-numbers technique, which limits mapping to these categories. Ecosystem maps are only used for general flight planning to ensure we adequately sample the ecosystem types that are believed to exist in a region.

The environmental variables used in the RFML models for each canopy trait were taken from co-aligned predictor spatial datasets (**Fig. S6**). We included a geological map of Peru (*31*). We incorporated three topographic variables – elevation, slope and aspect – derived from NASA Shuttle Radar Topography Mission (SRTM) data at 90 m resolution. A relative elevation model (a basic hydrological parameter we refer to as 'Hydro') was also developed from the SRTM data by calculating the height of the ground above the nearest water body (*42*), thus providing a spatial proxy for vegetation-related water resources. We also included mean annual precipitation (MAP) data derived from 12

years of NASA Tropical Rainfall Measurement Mission (TRMM) observations, as well as long-term (2000-2010) cloudiness data derived from the NASA Moderate Resolution Imaging Spectroradiometer (MODIS). Cloudiness is based on the number of times a MODIS pixel was identified as being affected by clouds in the Quality Assurance (QA) flags of the 8-day reflectance product. We included multiple potential incoming solar insolation models using SRTM elevation data in the SAGA GIS Potential Insolation module (www.saga-gis.org). These insolation layers (units of $kWhm^{-2}$) were created by modeling total insolation (direct and diffuse) for the days of the equinoxes and solstices (21^{st} of Mar, Jun, Sept, and Dec). We used Landsat imagery with the CLASlite forest mapping system only to define forest cover throughout the region, based on input maps of photosynthetic vegetation (PV), non-photosynthetic vegetation (NPV), and bare substrate cover (*43*). Environmental data maps were resampled to 1 ha resolution, co-aligned, and combined into a stack of predictor variables covering Andean and Amazonian forests of Peru.

Functional diversity classification

Following the derivation of the Peru-scale maps of seven canopy foliar traits, we used a K-means algorithm to integrate them as an ensemble indicating forest canopy functional diversity throughout the region. Before running the K-means algorithm, the values for each of the seven modeled foliar traits were scaled to unity, so that the statistical space was equally scaled in all dimensions. We used the *NbClust* package with Euclidean distance to determine the number of functionally unique classes (*44*). This algorithm uses up to 30 indices to determine the number of clusters in a dataset. Repeated (n = 75) production of the 30 indices indicated the existence of 36 functionally distinct forest types, hereafter referred to as *Forest Functional Classes* (**Fig. 2a**).

To further explore the spatial patterns of functional diversity, we condensed the resulting 36 *Forest Functional Classes* (FFC) into six groups, hereafter referred to as *Forest Functional Groups* (FFG), based on their relative similarity using hierarchical clustering of the mean foliar trait values in each class. Ward's clustering method was used for this step based on the mean standardized foliar trait maps. The convolution of 36 classes to six groups allowed us to more easily understand and report the geography of functional diversity with respect to those groups considered threatened, protected or unallocated according to government and non-government land-use allocation information compiled in a Geographic Information System (GIS).

Supplementary Text

Model verification

Seventy-nine 1-ha field plots (*21*) were used to check that the RFML-modeled canopy traits were in agreement with those estimated directly from airborne imaging spectroscopy (**Fig. S7**). Results indicate that canopy traits were generally modeled with good precision, as assessed with R^2 ($p < 0.05$) and Root Mean Squared Error (RMSE; σ) values relative to airborne imaging spectrometer-based estimates. We mapped the resulting uncertainty in each canopy trait by taking the square root of the sum of the squares of the calibration error (**Table S1**) and the geospatial modeling error (**Fig. S7**). This resulted in seven functional trait maps with estimated uncertainties of 4-24% at the 1-ha resolution scale (**Fig. S8**). These percentage uncertainties are small relative to ecological variability in canopy traits, both regionally (*19*) and globally in tropical forests (*14*). Nonetheless, these maps suggest geographies of relatively higher uncertainty among canopy traits, and indicate where additional airborne sampling could be carried out in the future.

Mapped trait inter-correlations

We tested inter-correlations between mapped forest canopy traits (**Fig. S9**). As predicted by leaf economics theory (*45*), foliar N was inversely correlated with leaf mass per area (LMA). Additional partial correlations were found between lignin and phenols (R = 0.50), and lignin and foliar Ca (R = -0.63). Overall however, the results show that most traits are not correlated. This indicates multi-dimensionality of the mapped traits, allowing for classifications of forest canopy functional diversity.

Environmental controls on forest canopy traits

We assessed the relative importance of environmental factors that contributed to the seven modeled and mapped forest canopy traits. To do so, we used RFML to quantify the relative importance of factors at the Peru scale. Results indicate that geologic substrate and elevation are the co-dominant controls, accounting for up to 60% of forest functional trait turnover (**Fig. 1**). Secondary contributions were individually made by topographic slope and lowland hydrology (relative elevation modeling). As a combination, however, solar insolation throughout the year accounted for up to 40% of functional trait variation throughout the region. We also assessed the proportion of the total trait variation accounted for by the model (map) parameters (67%-94%) (**Fig. 1**).

Forest functional classes and groups

The remotely sensed canopy trait classification based on K-means analysis resulted in 36 distinct *Forest Functional Classes* or FFC (**Fig. 2a; Table S2**). Hierarchical clustering of the 36 classes indicated six very broad groups, hereafter referred to as *Forest Functional Groups* (FFG), related by the seven mapped functional traits (**Fig. 2b; Fig. S10**). A set of maps is provided in **Figs. S11-S12** to show the location and extent of each FFG. The proportion of land area occupied by the 36 FFC grouped by the six FFG is provided in **Figs. S13**.

Patterns emerged among the FFCs and FFGs that were recognizable based on our long-term field studies and on information from the published literature. Here we narrate

our understanding of the six FFG, with reference to their contributing FFC, using data presented in **Figs. S11-S13**. We emphasize here that these classes transition between one another in various ways ranging, from abrupt transitions at the interface of different geologic substrates or hydrological regimes, to more gradual transitions based on elevation and climate factors.

FFG-1: Southern Amazonian lowlands and Fitzcarrald Arch: FFG-1 includes six FFC that together cover 13.4 million ha of the lowland Amazon. This forest group is strongly affected by the Nazca ridge of the Pacific plate that subducts the South American plate, causing uplift in a region of the southern lowland Peruvian Amazon known as the Fitzcarrald Arch (*46*). The Arch has generated a unique set of crest-valley features close to the Andes, and a portion of lowland forest that is raised ~300-450 m a.s.l. in an arch pattern emanating outward from the Andes in a northeastern direction towards the Peru-Brazil border. FFC-22 is located in the core of the Fitzcarrald Arch, and is characterized as having forest canopies with very high foliar P and Ca, high N, and very low LMA. Forests in this area inter-digitate with forests of lower but still elevated nutrient concentrations in FFC-21 that stretch off the edges of the Arch. Forest canopy biological diversity of the core FFC-22 portion of the Fitzcarrald Arch is poorly understood, but we do know that FFC-21 is comprised of a mix of tree canopies and bamboo forest (*47*). Moving outward from the interior portion of the Fitzcarrald Arch in the Amazonian lowlands, Arch-generated terraces (*terra firme*) have incised and eroded, providing transport of rock-derived nutrients to farther, outlying forests from the Fitzcarrald Arch (FFC-12 to 15).

FFG-2: Northern terra firme forests: In the northern Peruvian lowland Amazon, FFG-2 forests cover 15.4 million ha that harbor six FFC, some of which are separated by hundreds of kilometers. The far northwestern portion of this group (FFC-1, 4) is underlain by a mix of early to late Miocene substrates, including the Pebas and Nauta formations (*48*). Each of these substrates contains a unique forest composition that is strongly expressed in forest functional traits and soils (*49, 50*). FFG-2 contains also forests in the north-central eastern part of the lowlands that are dominated by FFC-3 and 17. These forests cover named regions such as Cordillera Azul and Sierra del Divisor, each with known unique forest canopy composition. In the western portion of FFG-2 along the Peru-Ecuador border, two additional and distinct FFC (2, 16) exist on basaltic substrates derived from volcanic activity in Ecuador. FFG-2 is generally characterized by very large forest canopy investments in defense (high LMA, phenols and lignin), but with distinctly different nutrient concentrations in each class within the group.

FFG-3: Northern and southern moist forests: FFG-3 covers 16.8 million ha, and is comprised of seven FFC spanning the entire north-south latitudes of the Peruvian lowland Amazon. This group is uniformly characterized by very high foliar Ca concentrations, moderate N and P, and very low investments in structural or chemical defense. Substrates throughout FFG-3 include vast areas of old (Miocene) and newer (Holocene) alluvial deposition (*51, 52*).

FFG-4: Amazonian colluvial deposition forests: Situated along the base of the Andes, FFG-4 contains five FFC covering a total of 9.1 million ha. These forests have canopies with relatively high foliar N and P, but very low foliar Ca concentrations. Investment in foliar defense is moderate relative to other forest functional groups. Within this group, FFC-23 to 25 rest on very nutrient-rich colluvium deposited from the Andes, and as a result, is well known as a region of intensive deforestation for agriculture (including oil palm plantations) and animal pastures (*24, 53*). In addition, FFC-35 and 36 are found on inactive, late-Holocene floodplains harboring nutrient-rich forests with unique canopy compositions (*52*).

FFG-5: Pastaza-Maranon Foreland Basin: FFG-5 covers 9.7 million ha and is comprised of five FFC. The ~100,000 km^2 Pastaza-Maranon Foreland Basin (PMFB) dominates this group, and is a vast subsiding peatland-fluvial system that receives sediments from surrounding Pastaza Fan, Andean, and Maranon river substrates. The PMFB is comprised of a variety of forest classes (FFC 19-20, 33, 34), each unique in floristic composition. Anoxic substrate conditions underpin the forest functional and compositional patterns expressed in our mapping results: This mosaic of forests has generally lower concentrations of canopy foliar nutrients and very large allocations to both physical (lignin, LMA) and chemical (phenols) defenses, as well as elevated leaf water concentrations. Other forest classes outside of, but hydrologically connected to, the PMFB within FFG-5 include wet forests on subsiding land surfaces (e.g., FFC-18).

FFG-6: Higher Andean forests: FFG-6 contains seven forest classes associated with sub-montane to montane environments in the Andes, along with areas of significant elevation (> 800 m) in the Andean-Amazonian forelands, for a total of 9.5 million ha. The northern and central Peruvian Andes are where granitic (north) and dolomite-dominated (central) surfaces are arranged in relatively gentle relief compared to the steeper southern Peruvian Andes. These surfaces are overlain by forests with high LMA and leaf water concentration, and low foliar N concentrations, as is found uniformly into the central and southern Andean forests. However, the northern and central Andean forests have higher canopy foliar N and phenol concentrations compared to southern Andean forests. Major changes in forest functional composition occurs by topographic slope (but not aspect), with higher nutrient canopies mapped in valley bottoms (e.g., FFC-26) relative to crests and steep slopes with weak soil nutrient retention, represented by classes such as FFC-28 and FFC-30. The sub-montane portion of this landscape contains another two or more functionally unique forest classes. The southern Peruvian Andes contain forests on more steeply inclined slopes compared to the northern and central Andean forests. These forest canopies have suppressed foliar P and enhanced lignin allocation, and also have diverse canopy nutrient distributions on crests and in valleys (FFC-29, 33). Southern Peruvian montane and sub-montane forests contain unique floristic and functional compositions (*19, 26, 54*).

Canopy traits at field plot and regional levels

We compared the mapped functional trait variation at the Andes-to-Amazon scale (**Table S2**) to the variation in 301 field inventory plots distributed in six watersheds across the Peruvian Andes-to-Amazon region **(Table S3)**. The location and description

of field plots, summarized by watershed, can be found in **Fig. S14** and **Tables S3-S4.** Remotely-sensed Ca and P accounted for the largest proportions of functional class variation, followed by LMA, as indicated by their large coefficients of variation **(Table S2)**. These most variable traits were followed by phenols and lignin, and then by foliar N and water concentration. Variation in the remotely-sensed canopy traits of the field inventory plots showed a pattern very similar to that of the entire region (**Table S3**). We again found that Ca and P were the most variable, followed by LMA, lignin and phenols. Foliar N and water concentrations were the least variable. Overall, these results suggest that remotely-sensed forest canopy trait variation within plots distributed among 32 of 36 mapped FFCs mirrors the variation observed among classes as a whole.

We used step-wise Regularized Discriminant Analysis (RDA) to test the efficacy of the FFC map to define the functional composition of the 301 field inventory plots. Of the 36 mapped classes, 32 classes contained at least one field plot (**Table S3**). The RDA method was selected to accommodate the unequal, and sometimes low number of plots within the 36 FFC. RDA analysis was performed on mean standardized values with $\lambda = 0.3$ and $\gamma = 0.5$. The lower λ decreases the restriction of linearity on the covariance matrix, and the neutral γ reduces the conformity to a diagonal covariance matrix, both of which were important to this dataset. Results indicated that the seven mapped canopy traits accurately defined the forest functional classes of the field plots throughout the network, with a $R^2 = 0.78$ (**Fig. S15**). All canopy traits contributed significantly to the model ($p < 0.001$), and were selected in the forward direction in the following order of importance, leaf water, leaf mass per area (LMA), P, Ca, phenols, N, and lignin (reverse selection removed traits in the opposite order). The combinatorial trait axes (canonical axes) as they relate to the seven foliar traits are given in **Table S5.**

Comparing floristic composition and remotely-sensed functional trait composition

To examine the multivariate relationship between floristic community composition and remotely-sensed canopy trait composition in the field plots, we used a non-metric multidimensional scaling (NMDS) approach based a Bray-Curtis dissimilarity matrix of species abundance to collapse the variation in the floristic data measured in the 301 field plots into a smaller set of dimensions (*55*). Floristic information for the field plots is provided in **Table S6**. We regressed the primary axis of community floristic composition (NMDS 1) with the primary axis of a principal components reduction of remotely-sensed canopy trait composition (**Fig S16**). Community floristic composition was inversely related ($y = -6.4x$) to foliar trait composition, and explained 43% of the remotely-sensed trait composition of the 301 field plots ($p < 0.001$). This finding further supports observed linkages between taxonomic and functional composition in Amazonian tree communities (*28, 48, 49, 56*).

Forest functional loss analysis

We analyzed forest functional diversity losses using deforestation data compiled by the Peruvian Ministry of Environment and the Carnegie Institution for Science for the period 2000 to 2014 (**Fig. S17**). These deforestation maps were generated from mosaicked

Landsat Thematic Mapper (TM) and Thematic Mapper+ (TM+) observations at 30-meter resolution, with a minimum mapping unit reporting at 1.0 ha resolution (*57*).

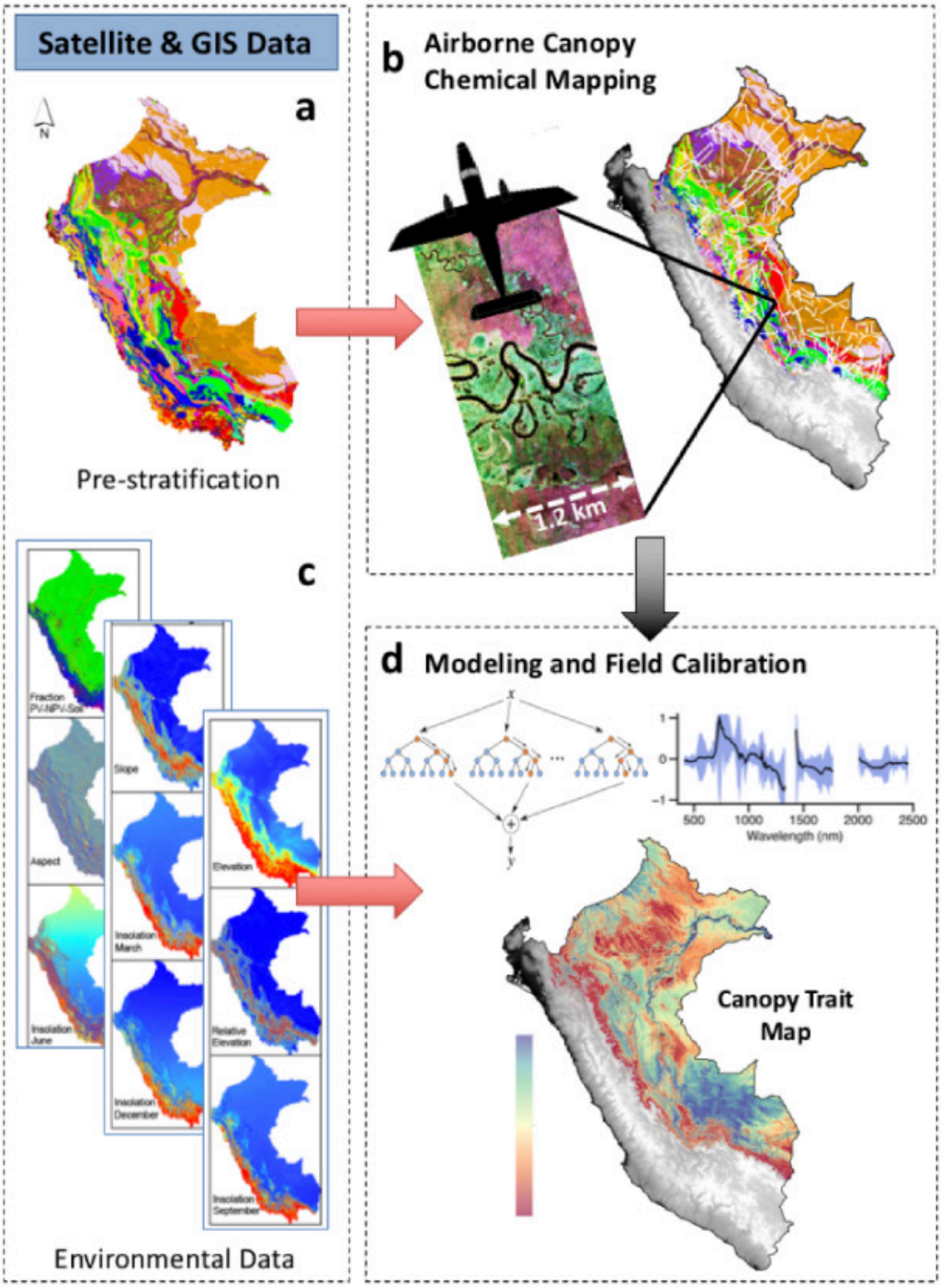

Fig. S1.

Overview of the methodology used to map forest canopy traits throughout the Peruvian Andes-to-Amazon region.

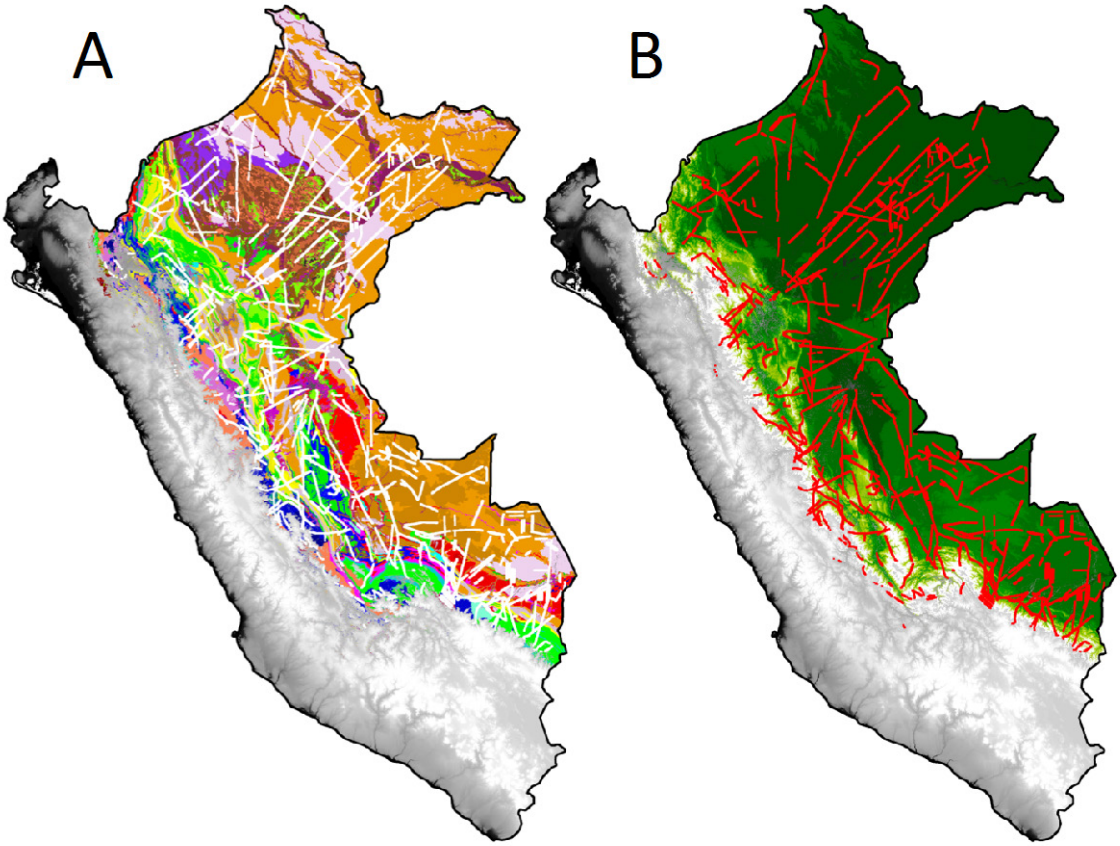

Fig. S2

Spatial distribution of Carnegie Airborne Observatory (CAO) flight lines, each 1.2 km in mapping swath, throughout the Andes-Amazon study region. The background maps are (a) geologic substrate and (b) elevation throughout the study region.

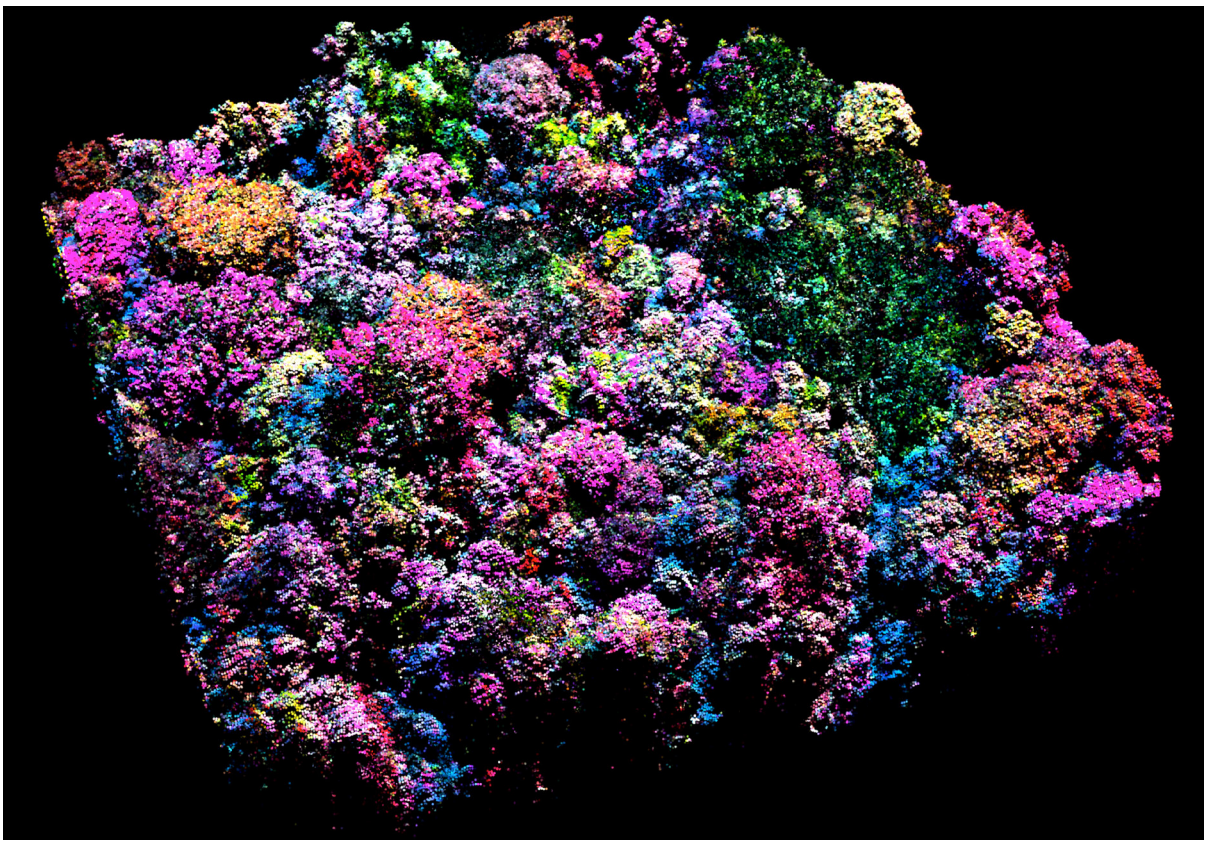

Fig. S3
Example single hectare of our 2,045,379 hectares of aircraft observations, demonstrating Carnegie Airborne Observatory (CAO) laser-guided imaging spectroscopy. Spectral data express chemical properties of each canopy individual down to leaf and branch levels. Colors here indicate changes in seven canopy traits (6 chemical + LMA) among co-existing individuals.

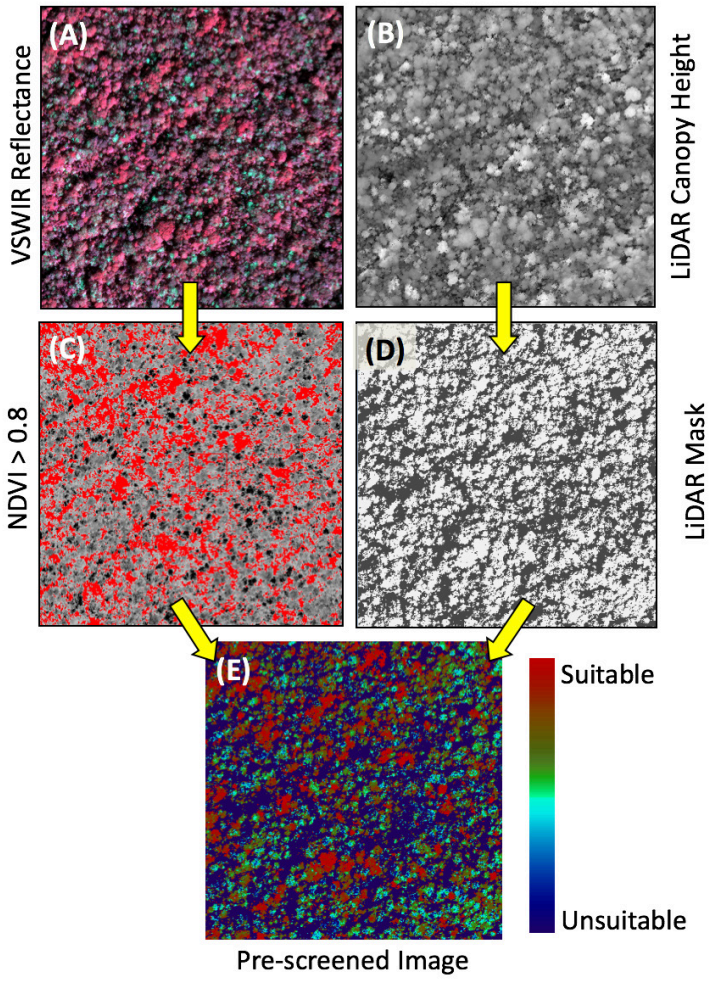

Fig. S4

Pre-screening of (a) CAO Visible-to-Shortwave Infrared (VSWIR) imaging spectrometer data using (b) embedded Light Detection and Ranging (LiDAR) data on canopy height and gaps. (c) Minimum NDVI threshold of 0.8 ensures sufficient foliar cover in each analysis pixel. (d) Combining LiDAR and solar-viewing geometry, a mask is generated to remove pixels in shade, and ground and water surfaces. (e) The resulting suitability image provides an indication of pixels that can be used for chemometric analysis, which are averaged at a spatial resolution of 1 ha.

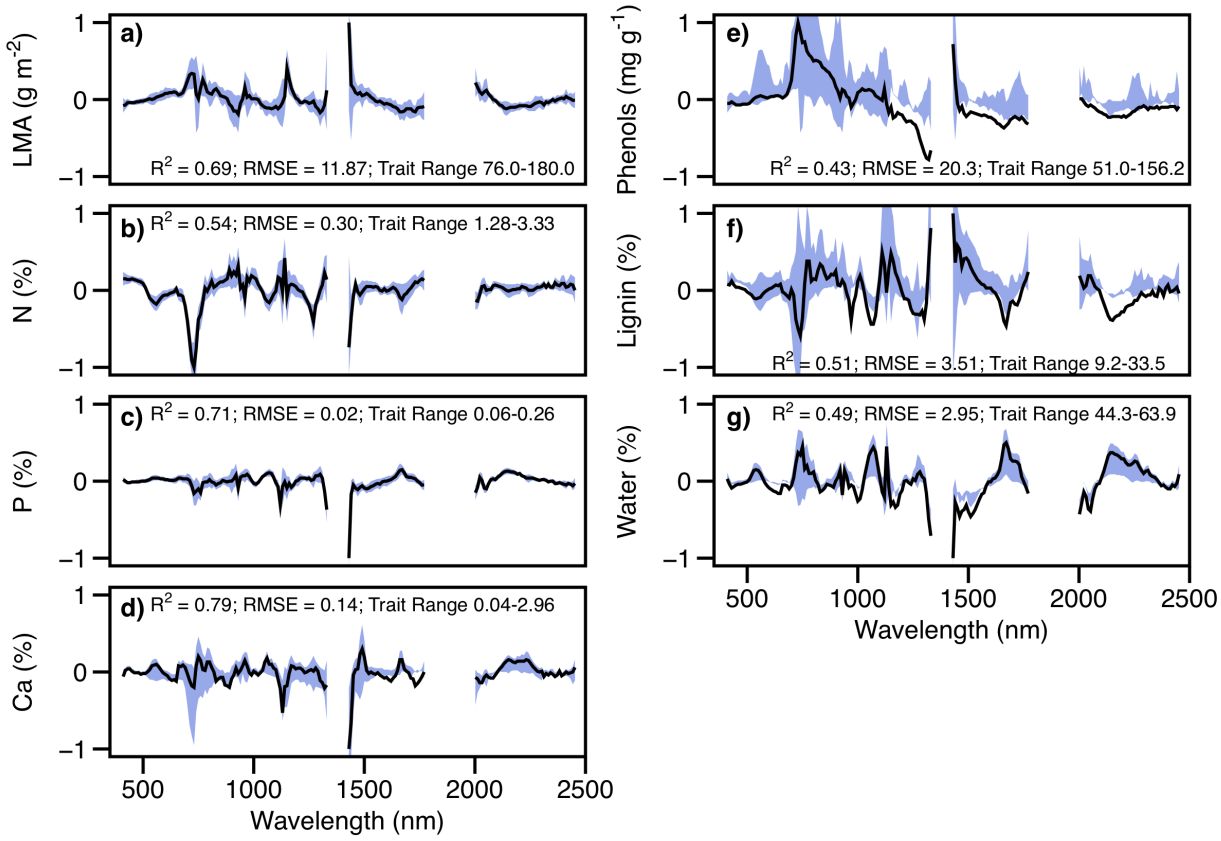

Fig. S5

Spectral dependence of leaf mass per unit area (LMA; a) and six canopy foliar chemical traits (b – g; N, P, Ca, phenols, lignin, and water respectively) along with the R^2, root mean square error (RMSE) derived from calibrations of laser-guided imaging spectrometer measurements at 1-ha resolution are given. The range in values for each trait among the 79 1-ha plots used for calibration (a portion of the field inventory plots) is included with their dependence graphs. The black line represents the mean dependence value and blue shading the standard deviation from the mean of the PLSR calibration runs.

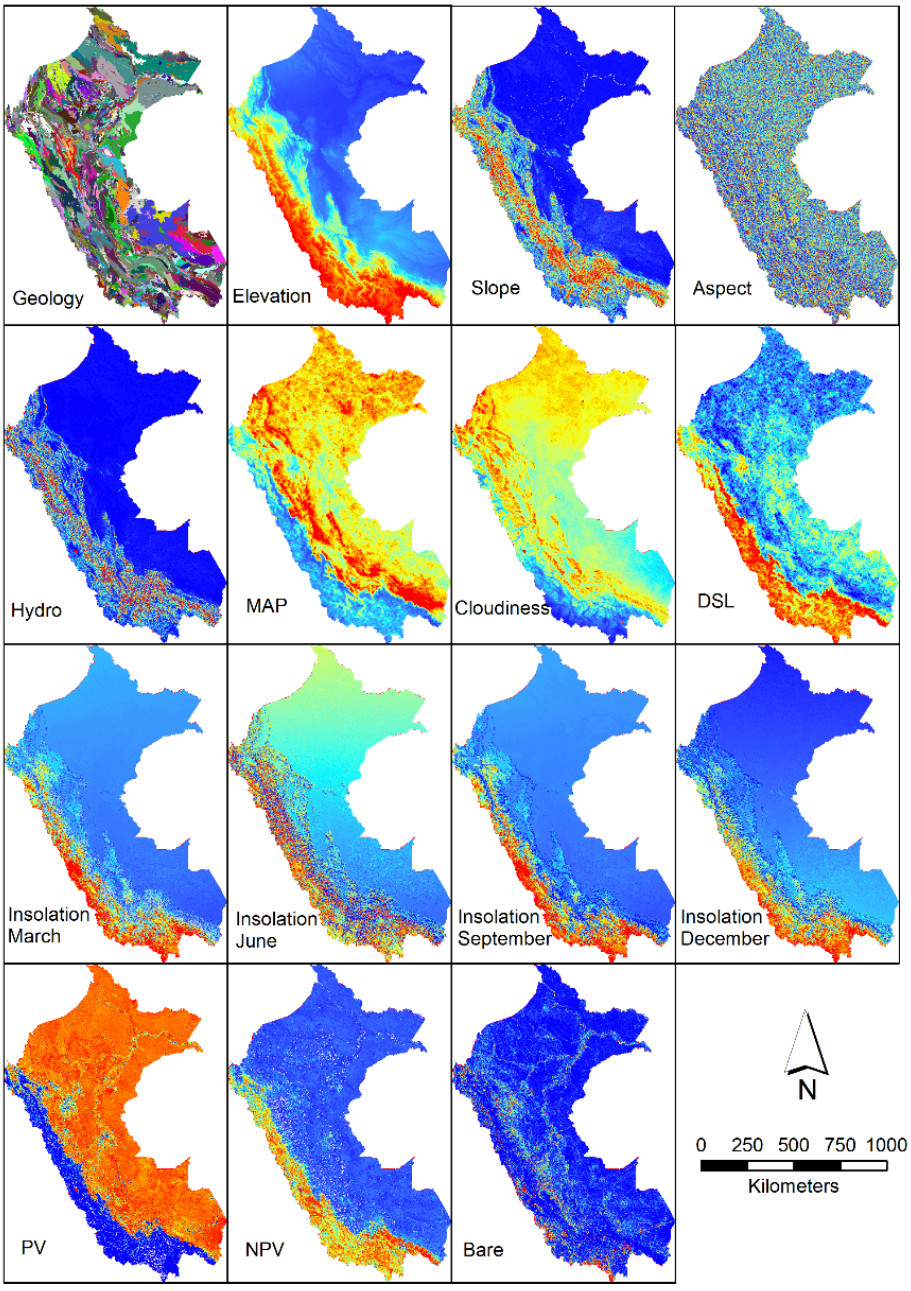

Fig. S6

Input data layers used for model-based upscaling of the airborne imaging spectrometer data. MAP = mean annual precipitation; DSL = day season length; PV = photosynthetic vegetation; NPV = non-photosynthetic vegetation; Bare = bare substrate (soils, rocks, etc.).

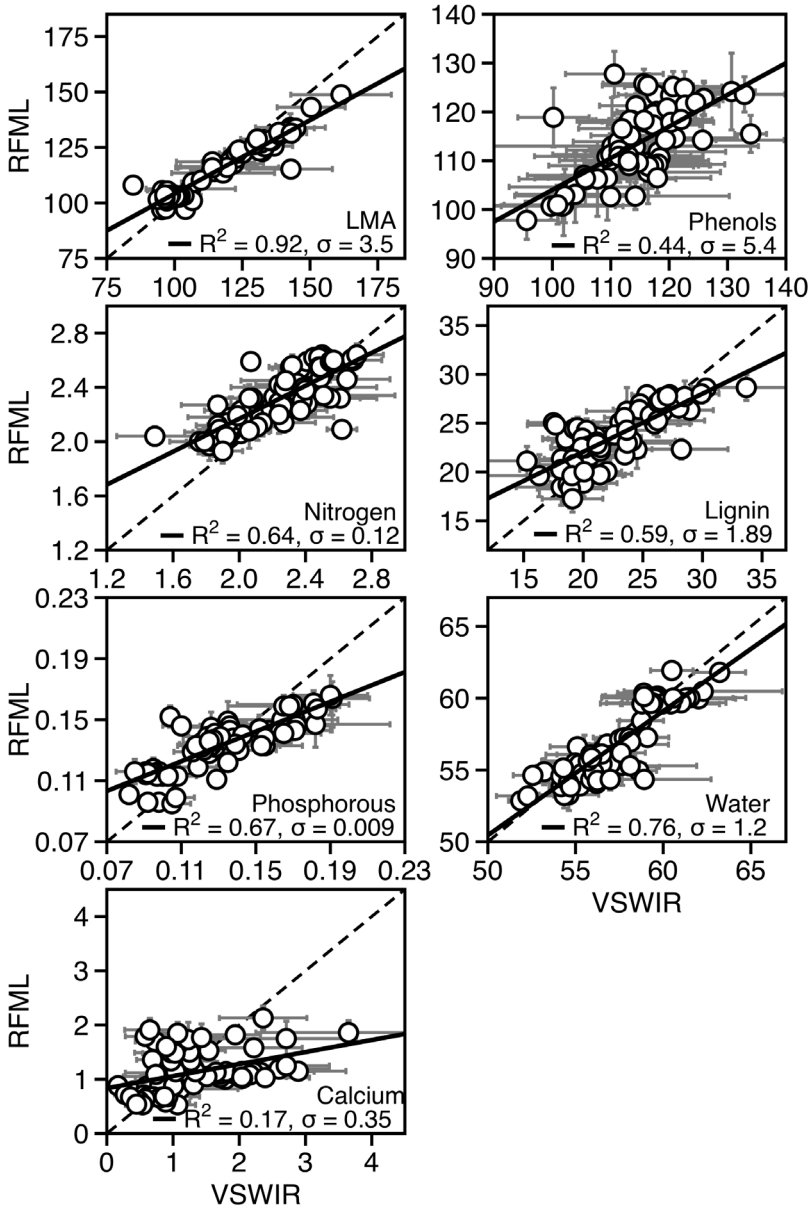

Fig. S7

Comparison of remotely sensed (VSWIR) and Random Forest Machine Learning (RFML)-modeled leaf mass per area (LMA) and foliar N, P, Ca, lignin, and water concentration at 79, 1-ha plots spread throughout the Peruvian Andes and Amazon region.

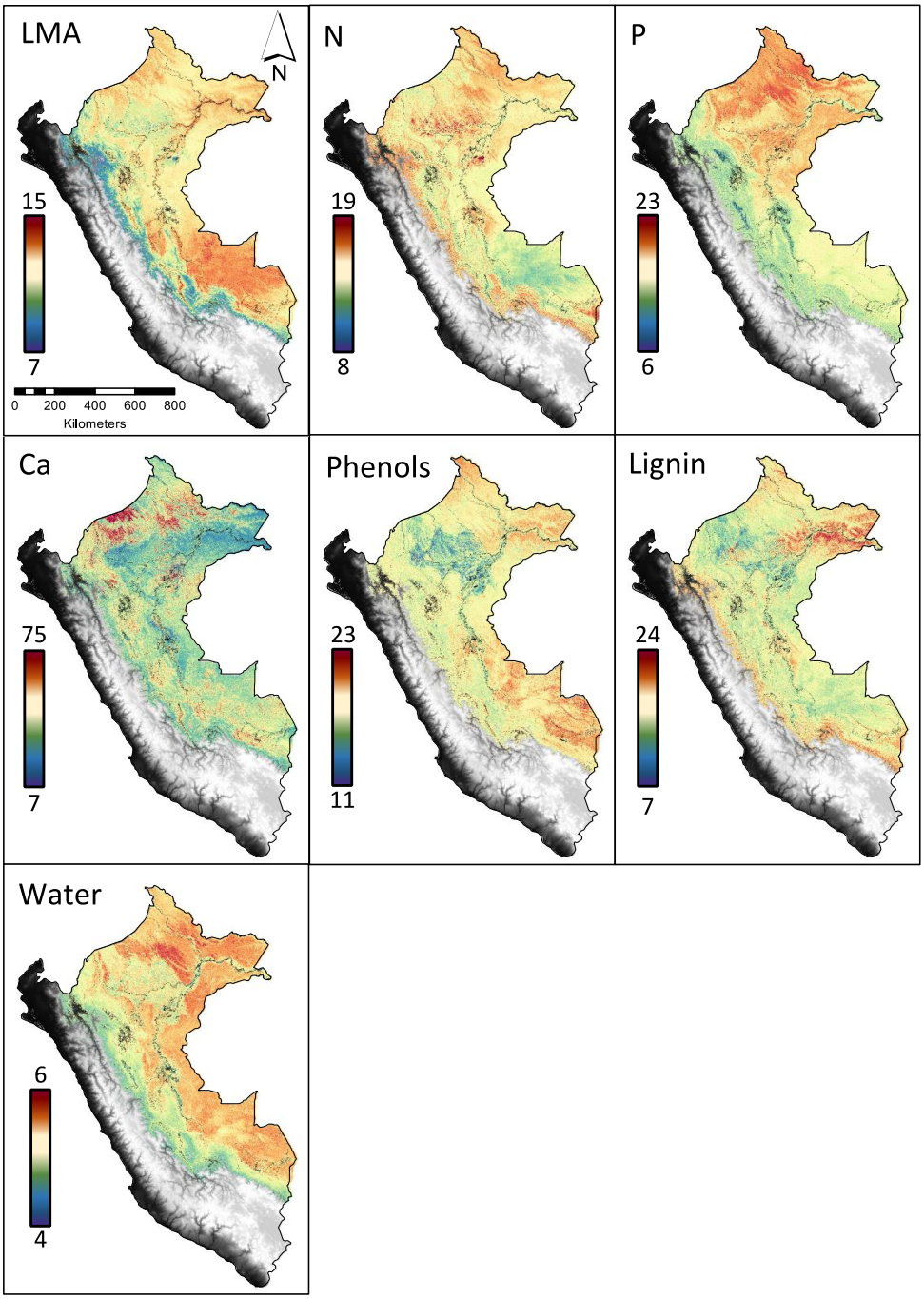

Fig. S8

Mapped accuracy for seven forest canopy traits throughout the Peruvian Amazon. Values are the square root of the sum of the squares of calibration error (**Table S1**) and geospatial modeling error, and are reported as a percentage of each grid cell value (**Fig. S7**).

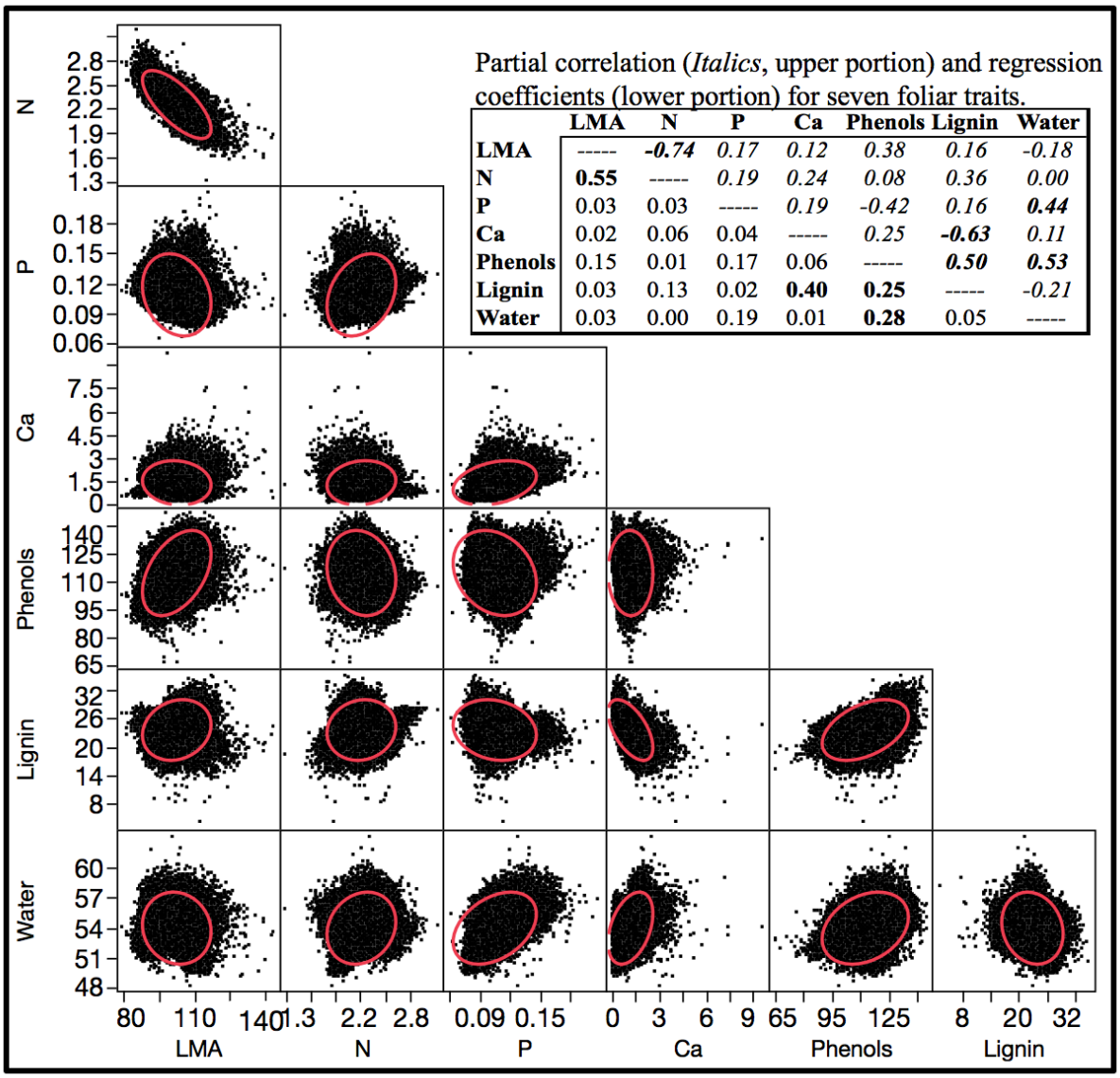

Fig. S9

Correlations and supporting statistics among the seven mapped forest canopy traits used for functional diversity classification.

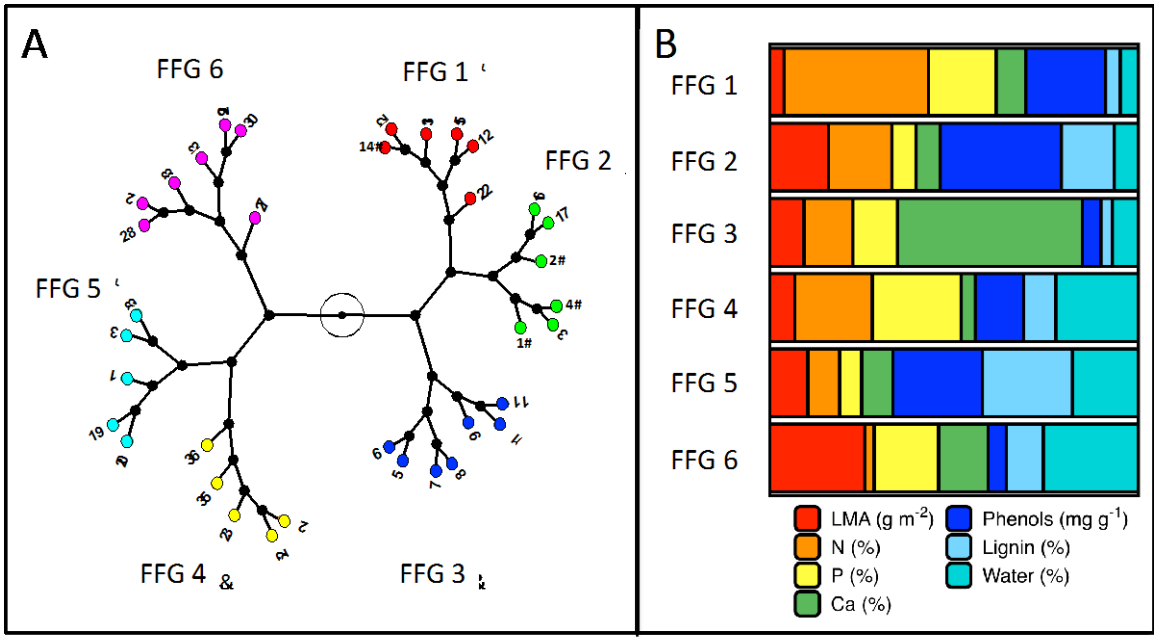

Fig. S10

a) Hierarchical clustering based on Ward's method of the mapped 36 forest functional classes (FFC) into six forest functional groups (FFG). Colors in the constellation diagram match those shown in **Fig S11**, and class numbers match those in **Fig. 2c** of main text. (b) Relative partitioning of forest canopy functional traits for each FFG, calculated from the mean canopy trait values each group and normalized to the total trait range among all groups.

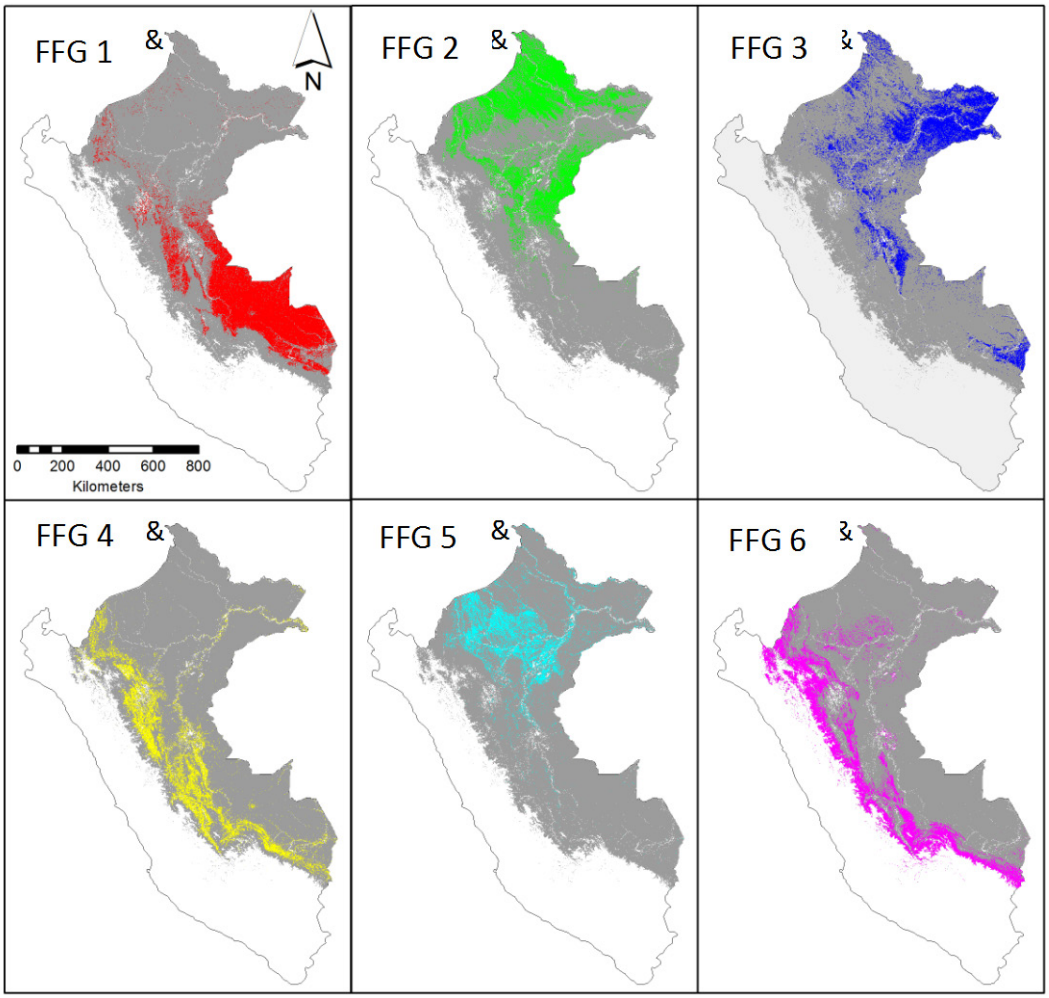

Fig. S11

Location and extent of six forest functional groups (FFG).

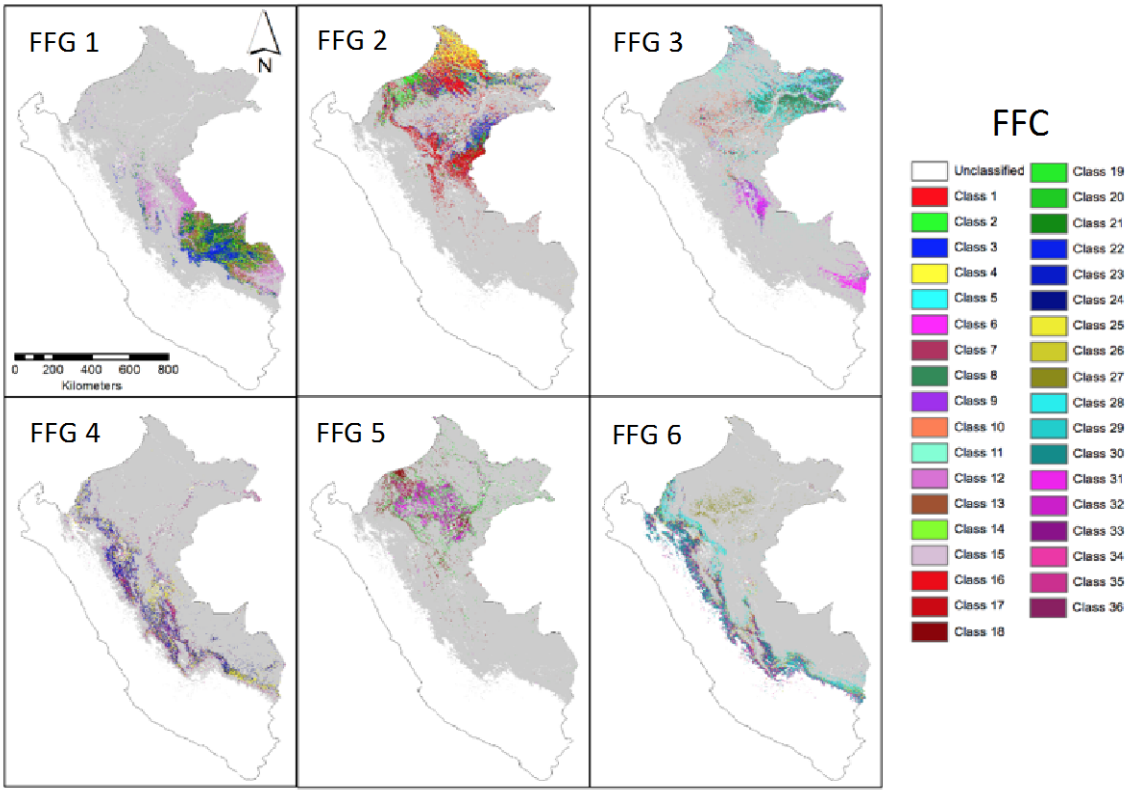

Fig. S12

Location and extent of 36 forest functional classes (FFC) sorted and displayed by forest functional groups (FFG).

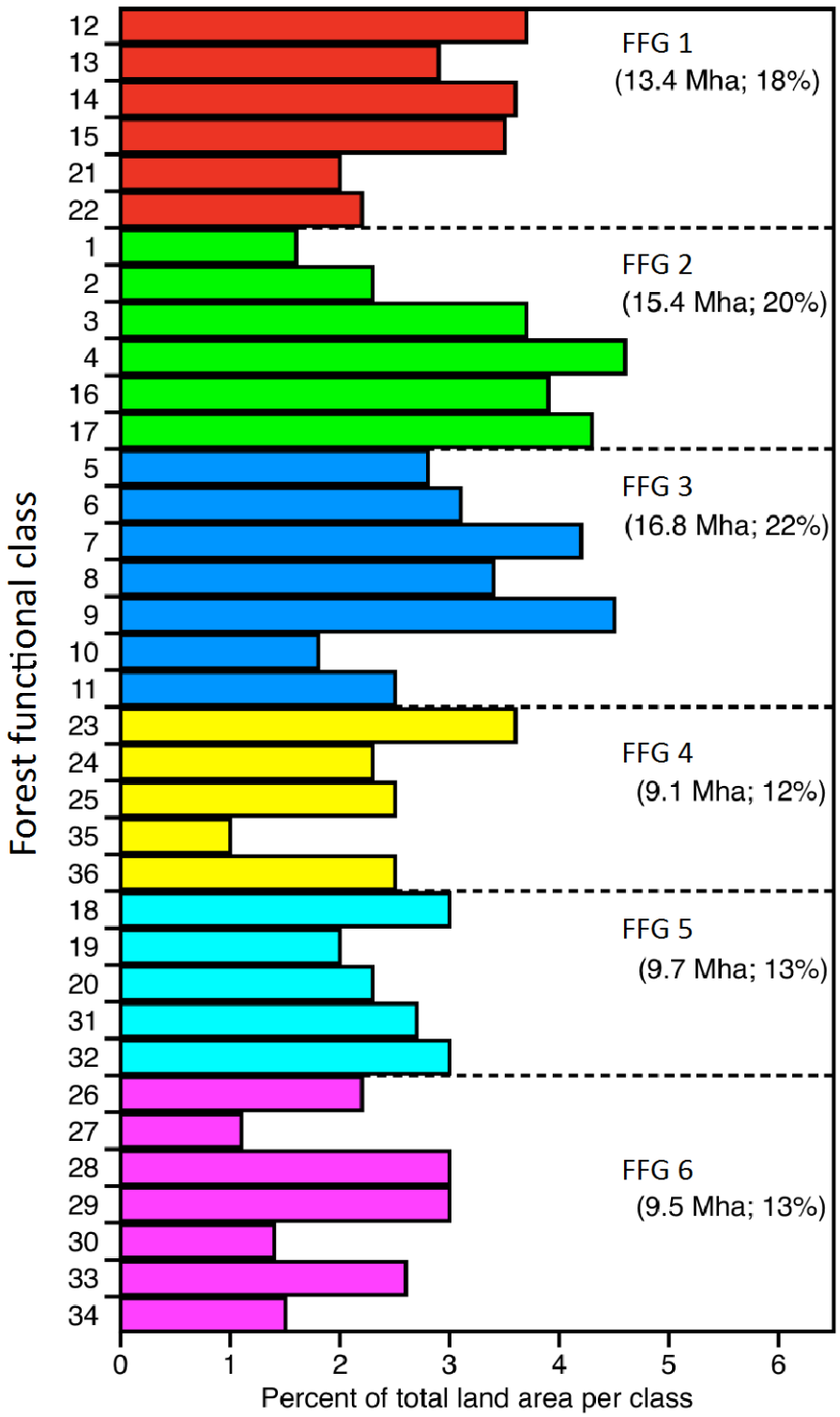

Fig. S13

Graph showing the proportion of land area in each functional forest class (FFC). The land area in each forest functional group (FFG) is shown in parentheses.

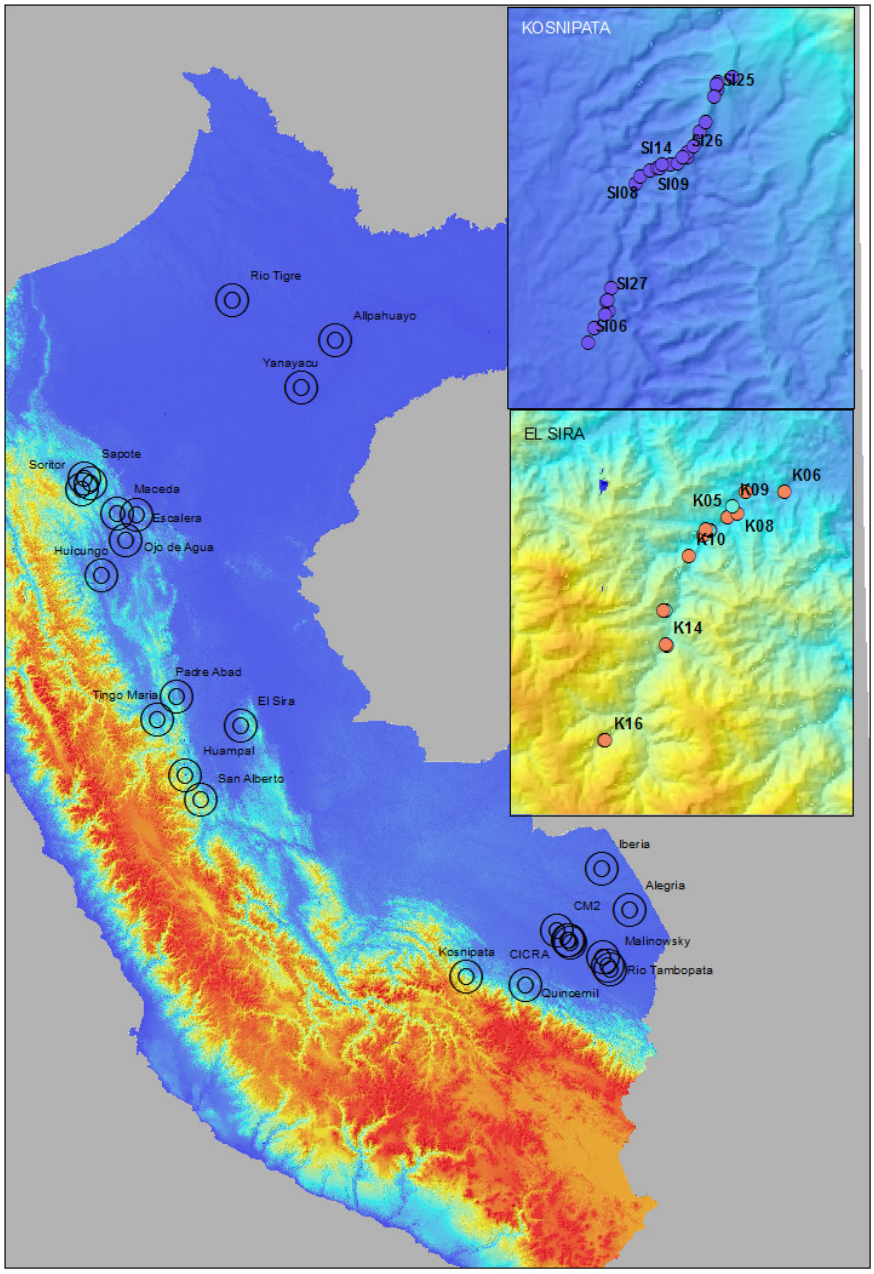

Fig. S14

General locations of our field plot network. Each circular symbol contains up to 40 0.3-ha field inventory plots.

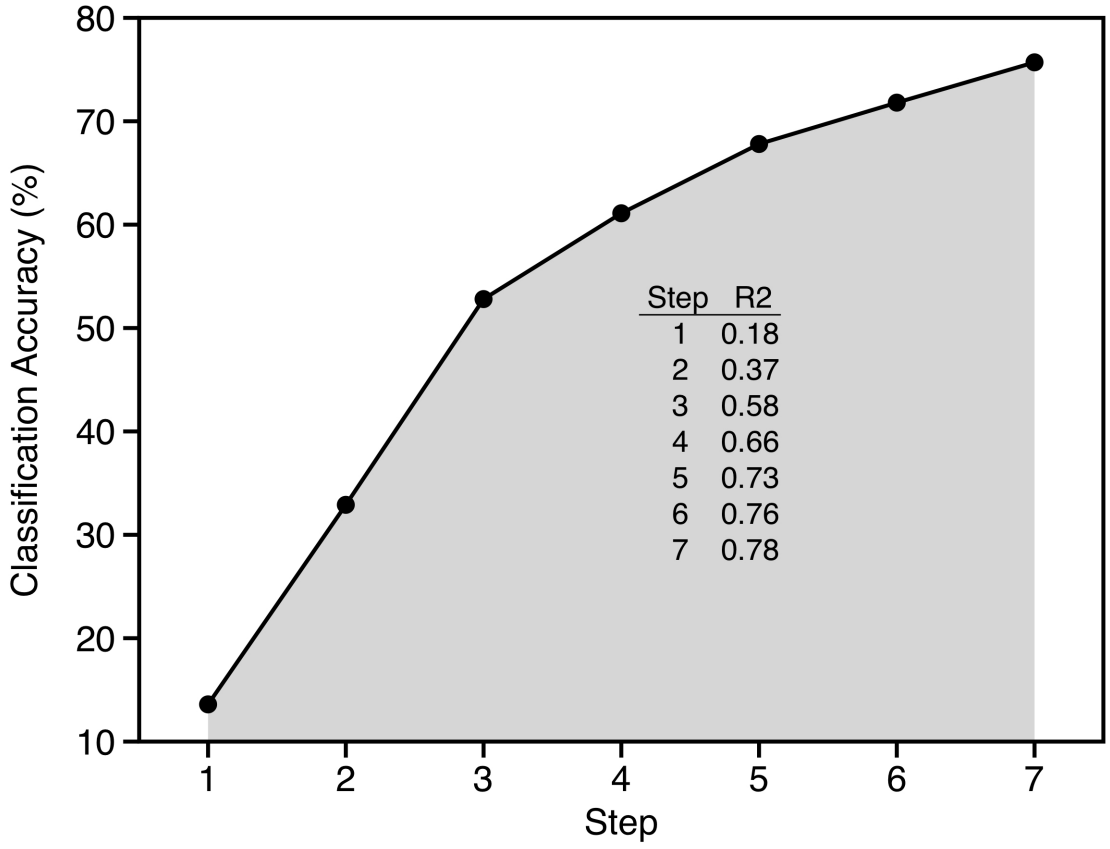

Fig. S15. Increase in the accuracy of Peru-wide functional diversity classification using forward step-wise regularized discriminant analysis (RDA) of seven remotely-sensed canopy chemical traits from 301 field plots. Canopy chemical traits were selected to enter the model in the following order, leaf water, leaf mass per area (LMA), P, Ca, phenols, N, and lignin, and all contributed significantly ($p < 0.001$).

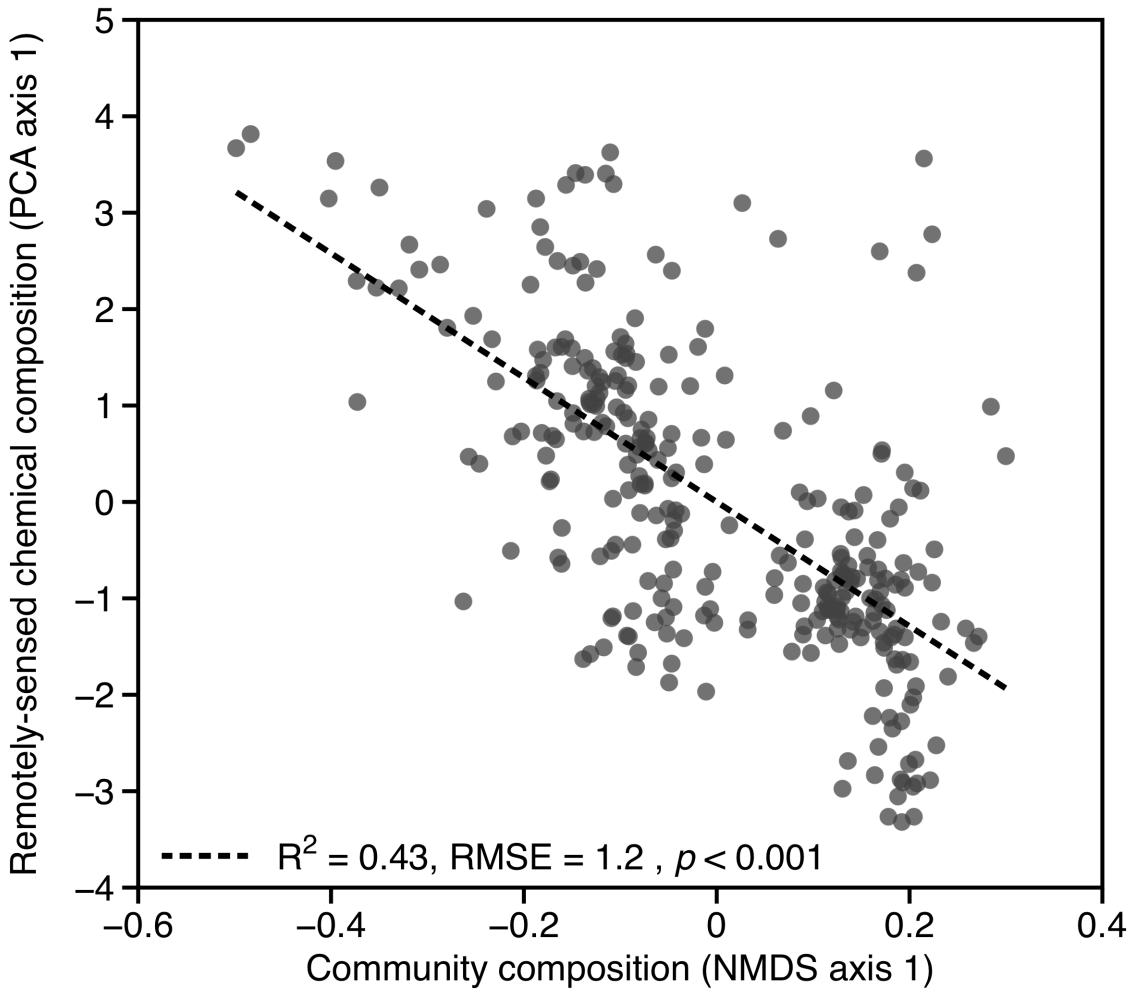

Fig. S16

Relationship between community composition and average remotely-sensed canopy foliar trait composition from 301 field plots spread across the Peruvian Amazon. Non-metric multidimensional scaling (NMDS) and principal components analysis (PCA) were used to reduce the abundance and foliar trait data respectively.

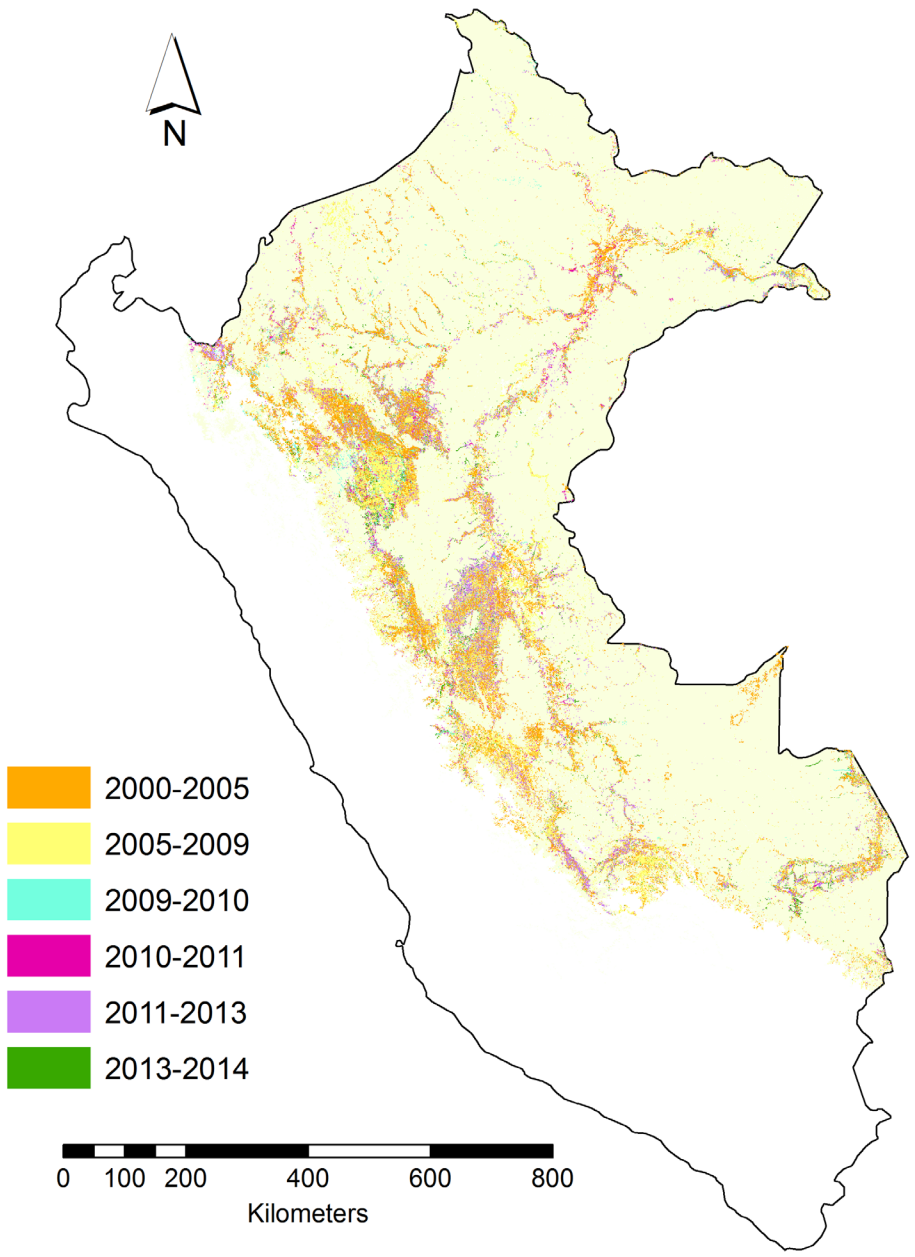

Fig. S17

Deforestation in the Peruvian Andes-Amazon region for the period 2000-2014.

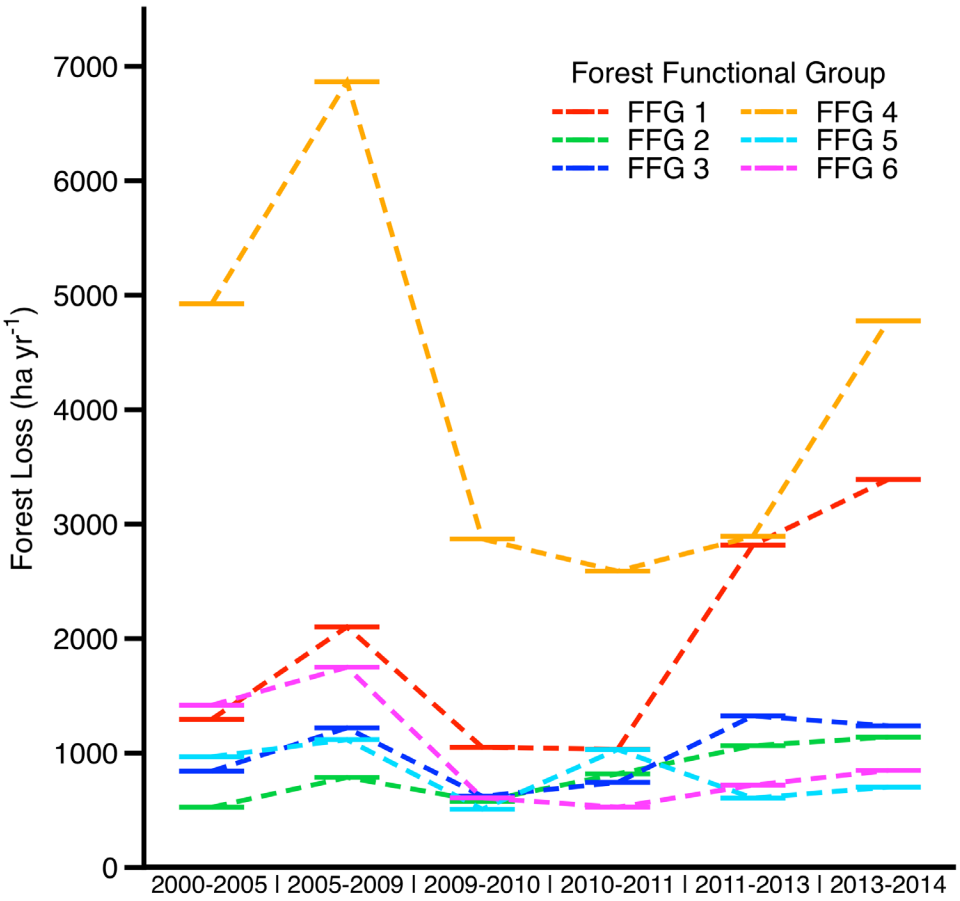

Fig. S18

Deforestation of mapped Forest Functional Groups (FFG) for the period 2000 to 2014.

Table S1.

Spectroscopic calibration of canopy chemical properties and leaf mass per area (LMA) using 1-ha filtered and brightness normalized airborne Visible-to-shortwave Infrared (VSWIR) spectroscopy.

	R^2	RMSE	%RMSE	Trait Range
LMA ($g\ m^{-2}$)	0.69±0.08	11.87±1.55	9.99	76.0-180.0
N (%)	0.54±0.09	0.30±0.03	14.47	1.28-3.33
P (%)	0.71±0.10	0.02±0.00	16.59	0.06-0.26
Ca (%)	0.79±0.17	0.14±0.06	16.99	0.04-2.96
Phenols ($mg\ g^{-1}$)	0.43±0.10	20.30±1.77	18.37	51.0-156.2
Lignin (%)	0.51±0.15	3.51±0.62	14.94	9.2-33.5
Water (%)	0.49±0.13	2.95±0.38	5.22	44.3-63.9

R^2 = regression coefficient for K-fold cross-validation data
RMSE = root mean square error in units of the original chemical assays
%RMSE = RMSE expressed as a percentage of the mean value of the leaf trait

Table S2.

Forest canopy trait values for 36 forest functional classes (FFC) in six forest functional groups (FFG), derived from airborne imaging spectroscopy and geostatistical modeling across the Peruvian Andes-Amazon region. Foliar traits include leaf mass per area (LMA, g m^{-2}), N (%), P (%), Ca (%), total phenols (mg g^{-1} dry leaf), lignin (%), and leaf water (%). Trait values are mean ± standard deviation. The range and coefficient of variation (CV) of the 36 class means for each trait are listed at the bottom of the table.

FFC (FFG)	Area (M ha)	LMA	N	P	Ca	Phenols	Lignin	Water
1 (2)	1.2	109.9±3.4	2.05±0.07	0.088±0.005	0.61±0.18	117.0±4.5	25.9±1.5	51.7±0.9
2 (2)	1.7	106.8±4.2	2.25±0.10	0.097±0.009	0.60±0.16	126.9±4.8	28.0±1.4	54.1±1.1
3 (2)	2.8	106.8±3.5	2.20±0.08	0.098±0.008	0.99±0.19	119.3±4.4	25.6±1.1	53.3±1.0
4 (2)	3.5	104.5±3.4	2.13±0.09	0.094±0.006	0.95±0.18	110.8±5.2	22.9±1.3	53.8±1.1
5 (3)	2.1	103.8±3.4	2.22±0.09	0.099±0.007	1.47±0.18	112.0±4.7	22.4±1.3	53.2±1.0
6 (3)	2.4	104.9±4.4	2.11±0.13	0.126±0.009	1.31±0.28	103.1±5.4	21.4±1.2	53.8±1.0
7 (3)	3.1	109.1±5.4	2.11±0.13	0.105±0.009	2.09±0.49	118.5±7.0	20.9±1.9	54.8±1.2
8 (3)	2.5	100.5±3.4	2.28±0.08	0.103±0.010	2.03±0.35	106.3±4.8	19.3±1.5	53.4±0.9
9 (3)	3.4	105.2±5.2	2.25±0.13	0.140±0.012	2.00±0.51	119.6±6.8	23.1±1.6	56.0±1.3
10 (3)	1.4	106.6±3.9	2.28±0.10	0.103±0.008	1.63±0.31	125.5±5.5	25.0±1.4	54.9±1.1
11 (3)	1.9	97.4±4.1	2.47±0.10	0.110±0.012	1.94±0.38	114.9±5.6	22.5±1.6	55.3±1.2
12 (1)	2.8	102.9±3.2	2.37±0.08	0.126±0.008	1.24±0.19	110.6±4.5	24.7±1.1	54.0±0.8
13 (1)	2.2	94.1±3.1	2.52±0.08	0.119±0.007	1.10±0.23	101.0±4.7	24.2±1.0	53.1±0.8
14 (1)	2.7	92.8±3.3	2.71±0.11	0.125±0.007	0.89±0.18	108.6±4.3	26.4±1.0	53.9±0.9
15 (1)	2.6	102.2±4.5	2.46±0.09	0.132±0.007	0.90±0.18	117.1±5.0	26.2±1.2	55.5±1.1
16 (2)	2.9	101.7±3.8	2.40±0.08	0.101±0.007	1.14±0.18	118.9±4.6	24.5±1.1	54.8±1.0
17 (2)	3.2	105.5±3.9	2.44±0.08	0.105±0.009	0.99±0.19	124.7±4.5	27.7±1.3	54.6±0.9
18 (5)	2.2	103.4±5.5	2.52±0.12	0.106±0.011	0.73±0.28	139.4±8.4	30.5±2.1	57.0±1.3
19 (5)	1.5	113.5±5.9	2.16±0.11	0.106±0.010	1.12±0.23	138.6±6.7	27.5±2.0	56.2±1.2
20 (5)	1.8	101.4±5.4	2.48±0.12	0.115±0.012	1.62±0.48	134.6±7.1	26.7±2.1	57.8±1.5
21 (1)	1.5	97.2±3.1	2.63±0.10	0.120±0.007	1.38±0.18	115.6±4.5	26.6±1.1	54.3±0.7
22 (1)	1.7	94.9±3.7	2.83±0.13	0.132±0.007	0.87±0.20	120.3±5.1	28.7±1.2	55.6±1.0
23 (4)	2.7	114.8±6.2	2.46±0.10	0.152±0.017	0.89±0.19	127.7±5.0	26.9±1.2	58.2±1.1
24 (4)	1.8	99.6±5.9	2.63±0.12	0.159±0.015	0.82±0.19	116.9±5.7	25.4±1.4	58.4±1.1
25 (4)	1.9	106.3±5.3	2.35±0.10	0.154±0.013	0.90±0.20	114.7±5.2	23.9±1.2	58.0±1.0
26 (6)	1.7	123.0±6.1	2.30±0.11	0.152±0.015	1.20±0.20	121.0±5.1	23.6±1.4	59.2±1.1
27 (6)	0.8	124.6±10.7	1.91±0.19	0.109±0.010	1.88±0.60	139.1±8.1	23.7±2.3	56.8±1.3
28 (6)	2.3	120.4±7.4	2.11±0.11	0.133±0.011	0.92±0.19	118.0±5.1	24.0±1.5	57.2±1.1
29 (6)	2.2	142.0±10.0	1.99±0.12	0.131±0.010	1.42±0.31	116.3±5.2	20.7±1.3	60.0±1.3
30 (6)	1.1	145.9±8.1	2.05±0.11	0.140±0.013	1.09±0.25	127.1±6.4	23.5±1.4	60.4±1.2
31 (5)	2.0	121.5±8.1	2.14±0.16	0.117±0.013	1.73±0.45	158.0±11.0	30.2±3.0	58.7±1.7
32 (5)	2.2	121.5±7.6	2.14±0.15	0.113±0.012	0.77±0.24	159.4±11.1	32.1±2.7	58.7±1.7
33 (6)	1.9	134.5±8.3	2.29±0.12	0.148±0.014	1.21±0.25	135.1±6.5	26.9±1.6	59.6±1.2
34 (6)	1.2	136.6±8.3	2.23±0.12	0.163±0.016	1.73±0.44	120.9±6.3	22.0±1.5	60.8±1.1
35 (4)	0.8	108.4±8.7	2.56±0.13	0.174±0.026	1.55±0.41	123.5±7.5	24.3±1.7	59.7±1.4
36 (4)	1.9	107.6±9.3	2.64±0.15	0.157±0.020	0.94±0.27	139.6±8.2	29.8±2.0	59.5±1.7
Range of class means		**92.8-145.9**	**1.91-2.83**	**0.088-0.174**	**0.60-2.09**	**101.0-159.4**	**19.3-32.1**	**51.7-60.8**
CV of class means		**12.1**	**9.4**	**18.3**	**34.3**	**10.8**	**11.6**	**4.5**

Table S3.

Forest canopy foliar traits mapped in 301 field inventory plots distributed throughout the Peruvian Andes-to-Amazon region. Functional diversity class (FFC) and group (G) are shown in parentheses and number of plots per class (#) is given. Foliar traits include leaf mass per area (LMA, g m^{-2}), N (%), P (%), Ca (%), total phenols (mg g^{-1}), lignin (%), and leaf water (%). Trait values are mean ± standard deviation. Also given, the average prediction probability (Prob.) and trait range for the plots matching the diversity class (Cl), as well as the range and coefficient of variation (CV) of class means. 'n' indicates no field plots in the class.

FFC (G)	#	Prob.	LMA	N	P	Ca	Phenols	Lignin	Water
1 (2)	2	1.00 (1.00-1.00)	108.7±1.1	2.08±0.04	0.088±0.002	1.08±0.49	117.7±4.5	25.4±2.1	51.1±0.1
2 (2)	n								
3 (2)	2	0.92 (0.87-0.98)	105.8±4.4	2.26±0.11	0.092±0.007	1.12±0.00	117.5±6.5	24.5±4.1	53.9±1.6
4 (2)	n								
5 (3)	8	0.73 (0.31-0.97)	102.9±1.5	2.27±0.05	0.107±0.010	1.78±0.43	112.9±6.4	21.8±2.1	53.0±0.6
6 (3)	3	0.70 (0.08-1.00)	103.7±3.0	2.25±0.10	0.129±0.008	1.23±0.25	100.5±5.6	22.1±1.1	53.9±1.0
7 (3)	n								
8 (3)	3	0.70 (0.18-1.00)	102.9±5.2	2.21±0.12	0.101±0.006	2.42±0.47	110.5±6.3	21.5±3.5	53.6±1.4
9 (3)	1	0.97	109.5	2.23	0.124	2.12	120.9	25.8	54.5
10 (3)	9	0.31 (0.01-0.61)	106.1±5.2	2.35±0.09	0.107±0.006	1.70±0.44	126.3±6.8	26.0±1.5	55.3±1.6
11 (3)	2	0.92 (0.86-0.99)	98.5±0.6	2.43±0.02	0.097±0.003	1.58±0.19	121.5±5.2	22.6±4.1	54.5±0.8
12 (1)	3	0.61 (0.04-0.94)	103.6±2.1	2.38±0.11	0.130±0.006	1.13±0.20	107.5±4.6	24.3±1.3	53.7±0.7
13 (1)	2	0.42 (0.01-0.93)	93.9±5.1	2.48±0.12	0.121±0.009	0.90±0.16	97.2±9.9	23.9±1.4	52.9±1.2
14 (1)	1	0.73 (0.44-0.94)	92.9±3.5	2.58±0.09	0.122±0.005	0.81±0.16	99.4±10.0	25.1±1.3	52.7±0.8
15 (1)	2	0.60 (0.01-0.95)	103.1±3.7	2.47±0.07	0.137±0.009	0.87±0.25	114.7±8.7	26.3±1.5	55.4±1.1
16 (2)	1	0.42 (0.06-0.79)	100.2±2.5	2.39±0.08	0.103±0.006	1.35±0.39	118.4±5.1	24.1±2.4	54.5±1.2
17 (2)	7	0.69 (0.22-0.95)	100.4±4.2	2.43±0.08	0.110±0.008	0.96±0.18	125.6±4.4	26.4±1.4	56.4±2.0
18 (5)	2	1.00 (0.99-1.00)	99.1±0.5	2.52±0.18	0.120±0.015	0.67±0.04	134.1±2.3	29.8±0.0	57.2±0.6
19 (5)	1	0.58	113.8	2.14	0.112	0.83	149.6	30.3	58.4
20 (5)	5	0.81 (0.60-0.96)	102.1±5.8	2.43±0.07	0.114±0.004	1.52±0.38	131.0±4.9	26.7±0.8	57.6±1.2
21 (1)	2	0.99 (0.98-1.00)	99.9±0.9	2.46±0.05	0.118±0.003	1.42±0.19	111.0±5.7	25.1±1.4	54.8±0.2
22 (1)	4	0.98 (0.94-1.00)	102.9±5.9	2.61±0.16	0.127±0.017	0.60±0.05	123.9±3.0	28.6±1.4	55.7±0.5
23 (4)	1	0.74 (0.00-1.00)	113.4±5.5	2.50±0.18	0.170±0.028	0.89±0.22	128.3±7.2	26.3±0.9	57.7±1.0
24 (4)	1	0.68 (0.14-0.98)	99.4±5.8	2.54±0.11	0.160±0.010	0.80±0.33	111.7±6.5	24.7±2.0	59.0±0.8
25 (4)	1	0.56 (0.01-0.98)	105.8±5.7	2.39±0.11	0.151±0.010	0.83±0.21	112.8±6.7	23.7±1.6	58.5±1.1
26 (6)	3	1.00 (0.99-1.00)	118.8±2.5	2.31±0.05	0.172±0.033	1.02±0.15	114.5±3.4	21.4±1.3	59.7±0.7
27 (6)	n								
28 (6)	3	0.85 (0.00-1.00)	118.5±5.5	2.09±0.13	0.128±0.008	0.97±0.15	116.7±4.9	24.0±1.4	57.7±1.0
29 (6)	3	0.87 (0.63-1.00)	136.6±5.8	2.11±0.14	0.135±0.010	1.44±0.24	118.1±9.1	21.5±2.1	60.4±2.0
30 (6)	3	0.99 (0.96-1.00)	148.5±2.2	2.04±0.11	0.137±0.008	1.26±0.05	125.0±2.7	22.0±1.3	60.5±1.0
31 (5)	2	0.67 (0.37-0.97)	111.3±5.7	2.23±0.10	0.109±0.010	1.92±0.36	131.8±13.0	26.2±2.8	55.5±1.7
32 (5)	2	0.98 (0.98-0.99)	114.4±0.1	2.16±0.04	0.113±0.004	0.65±0.19	157.7±1.6	31.5±2.3	58.8±0.5
33 (6)	5	0.65 (0.06-1.00)	126.5±13.6	2.24±0.15	0.151±0.012	1.08±0.27	135.8±11.3	26.7±3.1	60.1±1.8
34 (6)	7	0.94 (0.76-1.00)	137.0±9.2	2.23±0.10	0.163±0.011	1.51±0.28	121.2±5.7	21.2±0.8	60.6±0.7
35 (4)	1	0.96 (0.55-1.00)	118.5±5.3	2.60±0.13	0.179±0.015	1.79±0.40	122.5±4.3	24.2±1.3	59.4±0.8
36 (4)	7	0.45 (0.08-1.00)	105.3±5.7	2.58±0.21	0.151±0.021	0.83±0.22	128.7±12.4	28.5±2.7	58.3±0.8
Range		**0.76; 0.31-1.00**	**92.9-148.5**	**2.04-2.61**	**0.088-0.179**	**0.60-2.42**	**97.2-157.7**	**21.3-31.5**	**51.1-60.6**
CV			**11.7**	**7.1**	**19.0**	**37.2**	**10.7**	**10.7**	**4.8**

Table S4.
Distribution of 301field inventory plots by forest type and geologic substrate. Values indicate the number of plots per forest-geology combination.

		Geology[1]											
	Forest Type	Js-c	Ki-c	Kis-m	Nmp-c	NQ-c	P-c	Pali-ms	PN-c	Ps-c	Qh-c	Qpl-c	TsJi-m
Huallaga (26)													
Primary (22)	Restinga										1		
	Sclerophyllous				2								
	Submontane	15							3				
	Swamp										1		
Secondary (4)	Floodplain			1									
	Submontane				2		1						
Madre de Dios (113)													
Primary (86)	Floodplain										31		
	Mauritia Swamp										6	5	
	Montane							5					
	Submontane							8			8		
	Terrace										17	6	
Secondary (27)	Bamboo										1		
	Floodplain										1		
	Montane							1					
	Submontane							2			1		
	Terrace										12	9	
Maranon (23)													
Primary (18)	Floodplain										2	1	
	High Restinga					1						2	
	Low Restinga					1						1	
	Mauritia Swamp											3	
	Submontane												4
	Terrace					2					1		
Secondary (5)	High Restinga											1	
	Submontane												4
Nanay (41)													
Primary (25)	Chamizal											1	
	Terrace				8	2						2	
	Varillal				7	2						3	
Secondary (16)	Terrace				2	3							
	Varillal				7	2						2	
Tahuamanu (51)													
Primary (19)	Terrace											19	
Secondary (32)	Terrace											32	
Ucayali (47)													
Primary (42)	Montane									6			
	Submontane		24	9									3
Secondary (5)	Submontane			5									

[1]Geological abbreviations follow the official geologic map of Peru (*2*): Js-c , Jurasico superior continental.; Ki-c, Cretaceo inferior continental; Kis-m, Cretaceo inf.sup.Marino.; Nmp-c, Neogeno mioceno-continental.; NQ-c, Neogeno Cuaternario-continental.; P-c, Paleoceno continental; Pali-ms, Metased. del Paleozoico; PN-c, Paleogeno-Neogeno, Continental; Ps-c, Permico superior continental.; Qh-c, Cuaternario holoceno-continental.; Qpl-c, Cuaternario pleistoceno continental; TsJi-m, TriasicoSup,Jurasico inf.marino

Table S5.
Significant ($p < 0.05$) multivariate correlations among canonical scores and class-mean mapped canopy foliar traits across 301 field plots in the Peruvian Andes-to-Amazon region.

Canonical Score	Cumulative Variation (%)	LMA	N	P	Ca	Lignin	Phenols	Water
1	49	0.85	-0.24	0.65	ns	ns	0.50	0.92
2	67	0.38	-0.67	-0.67	0.51	-0.12	0.36	ns
3	81	-0.26	0.38	ns	-0.24	0.76	0.67	0.31
4	91	ns	0.38	0.22	0.78	-0.16	0.15	ns
5	96	0.24	0.13	ns	ns	0.51	0.37	-0.22
6	99	ns	-0.43	0.22	0.14	ns	ns	ns
7	100	ns	ns	-0.12	0.24	0.34	ns	ns

Table S6.
Floristic composition of 301 field plots in the Andes-Amazon region described by forest functional class (FFC). The number of plots and individuals in each FFC are given followed by the range (minimum and maximum) in number of families, genera and species in the plots within each FFC also the range in species abundance.

Forest Functional Class	Number of Plots	Individuals	Family	Genera	Species	Species Abundance
FFC-01	2	141	20-27	35-44	46-59	61-80
FFC-03	2	136	21-28	29-46	35-54	65-71
FFC-05	8	610	13-29	21-57	21-70	59-87
FFC-06	32	2334	3-26	3-55	3-65	25-111
FFC-08	3	279	10-29	12-53	14-62	78-121
FFC-09	1	75	11-11	16-16	16-16	75-75
FFC-10	9	666	7-26	11-51	14-57	37-127
FFC-11	2	132	18-26	34-43	39-55	63-69
FFC-12	35	2434	4-30	4-53	4-61	21-100
FFC-13	24	1359	12-24	18-46	18-46	29-85
FFC-14	11	707	14-26	22-45	22-46	38-93
FFC-15	24	1530	9-28	11-53	11-57	15-89
FFC-16	12	730	7-27	7-44	8-55	20-78
FFC-17	7	524	21-28	33-54	38-68	55-107
FFC-18	2	141	18-24	31-44	46-47	70-71
FFC-19	1	74	20-20	34-34	35-35	74-74
FFC-20	5	277	4-9	5-12	5-14	27-81
FFC-21	2	166	18-20	31-39	32-43	78-88
FFC-22	4	277	19-27	27-40	27-52	59-75
FFC-23	11	665	6-22	6-39	6-48	17-116
FFC-24	15	1021	4-28	4-49	4-60	6-106
FFC-25	17	1294	3-28	3-44	3-58	5-101
FFC-26	3	249	20-30	28-46	37-54	59-102
FFC-28	30	2796	6-30	7-52	7-61	50-135
FFC-29	3	260	17-19	19-23	20-34	56-119
FFC-30	3	264	12-19	14-26	17-34	73-114
FFC-31	2	184	4-11	6-15	6-17	62-122
FFC-32	2	126	10-18	18-35	21-35	49-77
FFC-33	5	443	8-19	9-31	11-36	66-124
FFC-34	7	700	13-27	15-36	17-41	73-122
FFC-35	10	642	11-22	20-34	23-37	48-101
FFC-36	7	491	4-24	5-41	5-55	50-104

Table S7.

Land area (M ha) of 36 Forest Functional Classes (FFC) arranged by Forest Functional Group (FFG) currently threatened, protected, or unallocated (opportunity lands). The percent of land area in each Class is provided in parentheses.

	FFC	Threats	Protections	Opportunities
FFG 1	12	1.78 (44%)	1.48 (37%)	0.75 (19%)
	13	0.92 (33%)	1.18 (42%)	0.70 (25%)
	14	0.82 (31%)	1.17 (44%)	0.68 (25%)
	15	1.01 (33%)	1.49 (48%)	0.58 (19%)
	21	0.76 (28%)	1.38 (50%)	0.60 (22%)
	22	0.91 (28%)	1.88 (57%)	0.52 (16%)
FFG 2	1	0.74 (32%)	0.86 (37%)	0.70 (30%)
	2	0.96 (35%)	1.02 (37%)	0.78 (28%)
	3	1.09 (28%)	1.54 (39%)	1.29 (33%)
	4	0.51 (17%)	1.01 (33%)	1.53 (50%)
	16	1.15 (35%)	1.09 (33%)	1.06 (32%)
	17	1.81 (42%)	1.68 (38%)	0.87 (20%)
FFG 3	5	0.78 (23%)	1.18 (35%)	1.44 (42%)
	6	0.63 (34%)	0.81 (44%)	0.40 (22%)
	7	0.30 (24%)	0.40 (32%)	0.55 (44%)
	8	0.74 (25%)	0.73 (25%)	1.50 (51%)
	9	0.35 (32%)	0.28 (26%)	0.46 (42%)
	10	0.65 (29%)	0.75 (34%)	0.84 (37%)
	11	0.38 (24%)	0.45 (28%)	0.78 (48%)
FFG 4	23	0.56 (24%)	1.12 (48%)	0.68 (29%)
	24	0.73 (34%)	0.77 (36%)	0.64 (30%)
	25	0.86 (32%)	1.03 (38%)	0.79 (30%)
	35	0.23 (19%)	0.35 (28%)	0.66 (53%)
	36	0.48 (27%)	0.81 (45%)	0.50 (28%)
FFG 5	18	0.66 (34%)	0.79 (41%)	0.47 (24%)
	19	0.42 (25%)	0.58 (35%)	0.65 (40%)
	20	0.42 (28%)	0.51 (34%)	0.56 (38%)
	31	0.29 (27%)	0.30 (28%)	0.50 (46%)
	32	0.37 (20%)	0.72 (39%)	0.77 (41%)
FFG 6	26	0.25 (16%)	0.63 (40%)	0.68 (44%)
	27	0.23 (25%)	0.27 (28%)	0.45 (47%)
	28	0.36 (21%)	1.03 (60%)	0.31 (18%)
	29	0.18 (7%)	0.68 (27%)	1.63 (66%)
	30	0.15 (6%)	0.77 (32%)	1.51 (62%)
	33	0.28 (17%)	0.72 (43%)	0.66 (40%)
	34	0.08 (4%)	0.40 (19%)	1.63 (77%)

References and Notes

1. S. H. Butchart, M. Walpole, B. Collen, A. van Strien, J. P. W. Scharlemann, R. E. A. Almond, J. E. M. Baillie, B. Bomhard, C. Brown, J. Bruno, K. E. Carpenter, G. M. Carr, J. Chanson, A. M. Chenery, J. Csirke, N. C. Davidson, F. Dentener, M. Foster, A. Galli, J. N. Galloway, P. Genovesi, R. D. Gregory, M. Hockings, V. Kapos, J.-F. Lamarque, F. Leverington, J. Loh, M. A. McGeoch, L. McRae, A. Minasyan, M. Hernández Morcillo, T. E. E. Oldfield, D. Pauly, S. Quader, C. Revenga, J. R. Sauer, B. Skolnik, D. Spear, D. Stanwell-Smith, S. N. Stuart, A. Symes, M. Tierney, T. D. Tyrrell, J.-C. Vié, R. Watson, Global biodiversity: Indicators of recent declines. *Science* **328**, 1164–1168 (2010). doi:10.1126/science.1187512 Medline

2. R. R. Nemani, S. W. Running, Satellite monitoring of global land cover changes and their impact on climate. *Clim. Change* **31**, 395–413 (1995). doi:10.1007/BF01095154

3. S. S. Saatchi, N. L. Harris, S. Brown, M. Lefsky, E. T. A. Mitchard, W. Salas, B. R. Zutta, W. Buermann, S. L. Lewis, S. Hagen, S. Petrova, L. White, M. Silman, A. Morel, Benchmark map of forest carbon stocks in tropical regions across three continents. *Proc. Natl. Acad. Sci. U.S.A.* **108**, 9899–9904 (2011). doi:10.1073/pnas.1019576108 Medline

4. R. B. Myneni, R. R. Nemani, S. W. Running, Estimation of global leaf area index and absorbed PAR using radiative transfer models. *IEEE Trans. Geosci. Remote Sens.* **35**, 1380–1393 (1997). doi:10.1109/36.649788

5. M. Loreau, Biodiversity and ecosystem functioning: A mechanistic model. *Proc. Natl. Acad. Sci. U.S.A.* **95**, 5632–5636 (1998). doi:10.1073/pnas.95.10.5632 Medline

6. C. Violle, P. B. Reich, S. W. Pacala, B. J. Enquist, J. Kattge, The emergence and promise of functional biogeography. *Proc. Natl. Acad. Sci. U.S.A.* **111**, 13690–13696 (2014). doi:10.1073/pnas.1415442111 Medline

7. D. U. Hooper, F. S. Chapin III, J. J. Ewel, A. Hector, P. Inchausti, S. Lavorel, J. H. Lawton, D. M. Lodge, M. Loreau, S. Naeem, B. Schmid, H. Setälä, A. J. Symstad, J. Vandermeer, D. A. Wardle, Effects of biodiversity on ecosystem functioning: A consensus of current knowledge. *Ecol. Monogr.* **75**, 3–35 (2005). doi:10.1890/04-0922

8. D. Tilman, F. Isbell, J. M. Cowles, Biodiversity and ecosystem functioning. *Annu. Rev. Ecol. Evol. Syst.* **45**, 471–493 (2014). doi:10.1146/annurev-ecolsys-120213-091917

9. A. von Humboldt, *Aspects of Nature in Different Lands and Different Climates* (Lea and Blanchard, 1850).

10. N. Myers, R. A. Mittermeier, C. G. Mittermeier, G. A. da Fonseca, J. Kent, Biodiversity hotspots for conservation priorities. *Nature* **403**, 853–858 (2000). doi:10.1038/35002501 Medline

11. H. Tuomisto, K. Ruokolainen, R. Kalliola, A. Linna, W. Danjoy, Z. Rodriguez, Dissecting Amazonian biodiversity. *Science* **269**, 63–66 (1995). doi:10.1126/science.269.5220.63 Medline

12. E. S. Gornish, C. M. Prather, Foliar functional traits that predict plant biomass response to warming. *J. Veg. Sci.* **25**, 919–927 (2014). doi:10.1111/jvs.12150

13. C. Field, H. A. Mooney, in *On the Economy of Plant Form and Function*, T. J. Givnish, Ed. (Cambridge Univ. Press, 1986), pp. 25–55.

14. G. P. Asner, R. E. Martin, Convergent elevation trends in canopy chemical traits of tropical forests. *Glob. Change Biol.* **22**, 2216–2227 (2016). doi:10.1111/gcb.13164 Medline

15. S. L. Ustin, D. A. Roberts, J. A. Gamon, G. P. Asner, R. O. Green, Using imaging spectroscopy to study ecosystem processes and properties. *Bioscience* **54**, 523–534 (2004). doi:10.1641/0006-3568(2004)054[0523:UISTSE]2.0.CO;2

16. P. D. Coley, J. A. Barone, Herbivory and plant defenses in tropical forests. *Annu. Rev. Ecol. Syst.* **27**, 305–335 (1996). doi:10.1146/annurev.ecolsys.27.1.305

17. R. F. Kokaly, G. P. Asner, S. V. Ollinger, M. E. Martin, C. A. Wessman, Characterizing canopy biochemistry from imaging spectroscopy and its application to ecosystem studies. *Remote Sens. Environ.* **113**, S78–S91 (2009). doi:10.1016/j.rse.2008.10.018

18. K. D. Chadwick, G. P. Asner, Organismic-scale remote sensing of canopy foliar traits in lowland tropical forests. *Remote Sens.* **8**, 87 (2016). doi:10.3390/rs8020087

19. G. P. Asner, R. E. Martin, R. Tupayachi, C. B. Anderson, F. Sinca, L. Carranza-Jiménez, P. Martinez, Amazonian functional diversity from forest canopy chemical assembly. *Proc. Natl. Acad. Sci. U.S.A.* **111**, 5604–5609 (2014). doi:10.1073/pnas.1401181111 Medline

20. A. R. Townsend, G. P. Asner, C. C. Cleveland, The biogeochemical heterogeneity of tropical forests. *Trends Ecol. Evol.* **23**, 424–431 (2008). doi:10.1016/j.tree.2008.04.009 Medline

21. G. P. Asner, R. E. Martin, C. B. Anderson, D. E. Knapp, Quantifying forest canopy traits: Imaging spectroscopy versus field survey. *Remote Sens. Environ.* **158**, 15–27 (2015). doi:10.1016/j.rse.2014.11.011

22. Materials and methods are available as supplementary materials.

23. C. A. J. Girardin, Y. Malhi, L. E. O. C. Aragão, M. Mamani, W. Huaraca Huasco, L. Durand, K. J. Feeley, J. Rapp, J. E. Silva-Espejo, M. Silman, N. Salinas, R. J. Whittaker, Net primary productivity allocation and cycling of carbon along a tropical forest elevational transect in the Peruvian Andes. *Glob. Change Biol.* **16**, 3176–3192 (2010). doi:10.1111/j.1365-2486.2010.02235.x

24. V. H. Gutiérrez-Vélez, R. DeFries, Annual multi-resolution detection of land cover conversion to oil palm in the Peruvian Amazon. *Remote Sens. Environ.* **129**, 154–167 (2013). doi:10.1016/j.rse.2012.10.033

25. G. P. Asner, W. Llactayo, R. Tupayachi, E. R. Luna, Elevated rates of gold mining in the Amazon revealed through high-resolution monitoring. *Proc. Natl. Acad. Sci. U.S.A.* **110**, 18454–18459 (2013). doi:10.1073/pnas.1318271110 Medline

26. M. R. Silman, in *Tropical Rain Forest Responses to Climate Change*, M. Bush, J. Flenley, W. D. Gosling, Eds. (Springer-Praxis, 2006), chap. 10, pp. 285–314.

27. B. Sakschewski, W. von Bloh, A. Boit, L. Poorter, M. Peña-Claros, J. Heinke, J. Joshi, K. Thonicke, Resilience of Amazon forests emerges from plant trait diversity. *Nat. Clim. Chang.* **6**, 1032–1036 (2016). doi:10.1038/nclimate3109

28. N. Fyllas, S. Patiño, T. R. Baker, G. Bielefeld Nardoto, L. A. Martinelli, C. A. Quesada, R. Paiva, M. Schwarz, V. Horna, L. M. Mercado, A. Santos, L. Arroyo, E. M. Jiménez, F. J. Luizão, D. A. Neill, N. Silva, A. Prieto, A. Rudas, M. Silviera, I. C. G. Vieira, G. Lopez-Gonzalez, Y. Malhi, O. L. Phillips, J. Lloyd, Basin-wide variations in foliar properties of Amazonian forest: Phylogeny, soils and climate. *Biogeosciences* **6**, 2677–2708 (2009). doi:10.5194/bg-6-2677-2009

29. O. E. Sala, F. S. Chapin 3rd, J. J. Armesto, E. Berlow, J. Bloomfield, R. Dirzo, E. Huber-Sanwald, L. F. Huenneke, R. B. Jackson, A. Kinzig, R. Leemans, D. M. Lodge, H. A. Mooney, M. Oesterheld, N. L. Poff, M. T. Sykes, B. H. Walker, M. Walker, D. H. Wall, Global biodiversity scenarios for the year 2100. *Science* **287**, 1770–1774 (2000). doi:10.1126/science.287.5459.1770 Medline

30. G. P. Asner, D. E. Knapp, J. Boardman, R. O. Green, T. Kennedy-Bowdoin, M. Eastwood, R. E. Martin, C. Anderson, C. B. Field, Carnegie Airborne Observatory-2: Increasing science data dimensionality via high-fidelity multi-sensor fusion. *Remote Sens. Environ.* **124**, 454–465 (2012). doi:10.1016/j.rse.2012.06.012

31. INGEMMET (Instituto Geologico Minero y Metalurgico, Peru), 2000; www.ingemmet.gob.pe/.

32. G. P. Asner, D. E. Knapp, R. E. Martin, R. Tupayachi, C. B. Anderson, J. Mascaro, F. Sinca, K. D. Chadwick, M. Higgins, W. Farfan, W. Llactayo, M. R. Silman, Targeted carbon conservation at national scales with high-resolution monitoring. *Proc. Natl. Acad. Sci. U.S.A.* **111**, E5016–E5022 (2014). doi:10.1073/pnas.1419550111 Medline

33. M. S. Colgan, C. A. Baldeck, J.-B. Féret, G. P. Asner, Mapping savanna tree species at ecosystem scales using support vector machine classification and BRDF correction on airborne hyperspectral and LiDAR data. *Remote Sens.* **4**, 3462–3480 (2012). doi:10.3390/rs4113462

34. G. P. Asner, D. E. Knapp, T. Kennedy-Bowdoin, M. O. Jones, R. E. Martin, J. Boardman, C. B. Field, Carnegie Airborne Observatory: In-flight fusion of hyperspectral imaging and waveform light detection and ranging for three-dimensional studies of ecosystems. *J. Appl. Remote Sens.* **1**, 013536 (2007). doi:10.1117/1.2794018

35. H. Feilhauer, G. P. Asner, R. E. Martin, S. Schmidtlein, Brightness-normalized partial least squares regression for hyperspectral data. *J. Quant. Spectrosc. Radiat. Transf.* **111**, 1947–1957 (2010). doi:10.1016/j.jqsrt.2010.03.007

36. G. P. Asner, R. E. Martin, D. E. Knapp, R. Tupayachi, C. Anderson, L. Carranza, P. Martinez, M. Houcheime, F. Sinca, P. Weiss, Spectroscopy of canopy chemicals in

humid tropical forests. *Remote Sens. Environ.* **115**, 3587–3598 (2011). doi:10.1016/j.rse.2011.08.020

37. D. M. Haaland, E. V. Thomas, Partial least-squares methods for spectral analyses. 1. Relation to other quantitative calibration methods and the extraction of qualitative information. *Anal. Chem.* **60**, 1193–1202 (1988). doi:10.1021/ac00162a020

38. A.-L. Boulesteix, K. Strimmer, Partial least squares: A versatile tool for the analysis of high-dimensional genomic data. *Brief. Bioinform.* **8**, 32–44 (2007). doi:10.1093/bib/bbl016 Medline

39. H. Martens, Reliable and relevant modelling of real world data: A personal account of the development of PLS Regression. *Chemom. Intell. Lab. Syst.* **58**, 85–95 (2001). doi:10.1016/S0169-7439(01)001 53-8

40. L. Breiman, Random forests. *Mach. Learn.* **45**, 5–32 (2001). doi:10.1023/A:1010933404324

41. J. S. Evans, M. A. Murphy, Z. A. Holden, S. A. Cushman, in *Predictive Species and Habitat Modeling in Landscape Ecology: Concepts and Applications*, C. A. Drew, Y. F. Wiersma, F. Huettmann, Eds. (Springer Science, 2011), pp. 139–159.

42. J. Mascaro, G. P. Asner, D. E. Knapp, T. Kennedy-Bowdoin, R. E. Martin, C. Anderson, M. Higgins, K. D. Chadwick, A tale of two "forests": Random forest machine learning aids tropical forest carbon mapping. *PLOS ONE* **9**, e85993 (2014). doi:10.1371/journal.pone.0085993 Medline

43. G. P. Asner, D. E. Knapp, A. Balaji, G. Paez-Acosta, Automated mapping of tropical deforestation and forest degradation: CLASlite. *J. Appl. Remote Sens.* **3**, 033543 (2009). doi:10.1117/1.3223675

44. M. Charrad, N. Ghazzali, V. Boiteau, A. Niknafs, An R package for determining the relevant number of clusters in a data set. *J. Stat. Softw.* **61**, 1–15 (2014). doi:10.18637/jss.v061.i06

45. I. J. Wright, P. B. Reich, M. Westoby, D. D. Ackerly, Z. Baruch, F. Bongers, J. Cavender-Bares, T. Chapin, J. H. C. Cornelissen, M. Diemer, J. Flexas, E. Garnier, P. K. Groom, J. Gulias, K. Hikosaka, B. B. Lamont, T. Lee, W. Lee, C. Lusk, J. J. Midgley, M.-L. Navas, U. Niinemets, J. Oleksyn, N. Osada, H. Poorter, P. Poot, L. Prior, V. I. Pyankov, C. Roumet, S. C. Thomas, M. G. Tjoelker, E. J. Veneklaas, R. Villar, The worldwide leaf economics spectrum. *Nature* **428**, 821–827 (2004). doi:10.1038/nature02403 Medline

46. V. Regard, R. Lagnous, N. Espurt, J. Darrozes, P. Baby, M. Roddaz, Y. Calderon, W. Hermoza, Geomorphic evidence for recent uplift of the Fitzcarrald Arch (Peru): A response to the Nazca Ridge subduction. *Geomorphology* **107**, 107–117 (2009). doi:10.1016/j.geomorph.2008.12.003

47. A. L. de Carvalho, B. W. Nelson, M. C. Bianchini, D. Plagnol, T. M. Kuplich, D. C. Daly, Bamboo-dominated forests of the southwest Amazon: Detection, spatial extent, life cycle length and flowering waves. *PLOS ONE* **8**, e54852 (2013). doi:10.1371/journal.pone.0054852 Medline

48. M. A. Higgins, K. Ruokolainen, H. Tuomisto, N. Llerena, G. Cardenas, O. L. Phillips, R. Vásquez, M. Räsänen, Geological control of floristic composition in Amazonian forests. *J. Biogeogr.* **38**, 2136–2149 (2011). doi:10.1111/j.1365-2699.2011.02585.x Medline

49. M. A. Higgins, G. P. Asner, C. B. Anderson, R. E. Martin, D. E. Knapp, R. Tupayachi, E. Perez, N. Elespuru, A. Alonso, Regional-scale drivers of forest structure and function in northwestern Amazonia. *PLOS ONE* **10**, e0119887 (2015). doi:10.1371/journal.pone.0119887 Medline

50. H. Tuomisto, K. Ruokolainen, M. Yli-Halla, Dispersal, environment, and floristic variation of western Amazonian forests. *Science* **299**, 241–244 (2003). doi:10.1126/science.1078037 Medline

51. C. Hoorn, F. P. Wesselingh, H. ter Steege, M. A. Bermudez, A. Mora, J. Sevink, I. Sanmartín, A. Sanchez-Meseguer, C. L. Anderson, J. P. Figueiredo, C. Jaramillo, D. Riff, F. R. Negri, H. Hooghiemstra, J. Lundberg, T. Stadler, T. Särkinen, A. Antonelli, Amazonia through time: Andean uplift, climate change, landscape evolution, and biodiversity. *Science* **330**, 927–931 (2010). doi:10.1126/science.1194585 Medline

52. G. P. Asner, C. B. Anderson, R. E. Martin, R. Tupayachi, D. E. Knapp, F. Sinca, Landscape biogeochemistry reflected in shifting distributions of chemical traits in the Amazon forest canopy. *Nat. Geosci.* **8**, 567–573 (2015). doi:10.1038/ngeo2443

53. C. Staver, Why farmers rotate fields in maize-cassava-plantain bush fallow agriculture in the wet Peruvian Amazon. *Hum. Ecol.* **17**, 401–426 (1989). doi:10.1007/BF00889498

54. K. J. Feeley, M. R. Silman, M. B. Bush, W. Farfan, K. G. Cabrera, Y. Malhi, P. Meir, N. S. Revilla, M. N. R. Quisiyupanqui, S. Saatchi, Upslope migration of Andean trees. *J. Biogeogr.* **38**, 783–791 (2011). doi:10.1111/j.1365-2699.2010.02444.x

55. J. Oksanen *et al.*, R package vegan: Community Ecology Package. Version XX (R Foundation for Statistical Computing, 2015); https://CRAN.R-project.org/package=vegan.

56. H. ter Steege, N. C. A. Pitman, O. L. Phillips, J. Chave, D. Sabatier, A. Duque, J.-F. Molino, M.-F. Prévost, R. Spichiger, H. Castellanos, P. von Hildebrand, R. Vásquez, Continental-scale patterns of canopy tree composition and function across Amazonia. *Nature* **443**, 444–447 (2006). doi:10.1038/nature05134 Medline

57. W. Llactayo, K. Salcedo, E. Victoria, "Memoria técnica de la cuantificación de los cambios de la cobertura de bosque a no bosque por deforestación en el ambito de la Amazonía Peruana (periodo 2009-2010-2011)" (Peruvian Ministry of Environment, 2013).